

Nucleosynthesis Yields of Core-Collapse Supernovae and Hypernovae, and Galactic Chemical Evolution

Ken'ichi Nomoto^a Nozomu Tominaga^a Hideyuki Umeda^a
Chiaki Kobayashi^b Keiichi Maeda^c

^a*Department of Astronomy, University of Tokyo, Bunkyo-ku, Tokyo 113-0033,
Japan*

^b*National Astronomical Observatory, Mitaka, Tokyo, Japan*

^c*Department of Earth Science and Astronomy, College of Arts and Science,
University of Tokyo, Meguro-ku, Tokyo 153-8902, Japan*

*To appear in Nuclear Physics A (Special Issue on Nuclear Astrophysics)
eds. K. Langanke, F.-K. Thielemann, & M. Wiescher (2006)*

Abstract

We present new nucleosynthesis yields as functions of the stellar mass, metallicity, and explosion energy (corresponding to normal supernovae and Hypernovae). We apply the results to the chemical evolution of the solar neighborhood. Our new yields are based on the new developments in the observational/theoretical studies of supernovae (SNe) and extremely metal-poor (EMP) stars in the halo, which have provided excellent opportunities to test the explosion models and their nucleosynthesis. We use the light curve and spectra fitting of individual SN to estimate the mass of the progenitor, explosion energy, and produced ^{56}Ni mass. Comparison with the abundance patterns of EMP stars has made it possible to determine the model parameters of core-collapse SNe, such as mixing-fallback parameters.

More specifically, we take into account the two distinct new classes of massive SNe: 1) very energetic Hypernovae, whose kinetic energy (KE) is more than 10 times the KE of normal core-collapse SNe, and 2) very faint and low energy SNe (Faint SNe). These two new classes of SNe are likely to be “black-hole-forming” SNe with rotating or non-rotating black holes. Nucleosynthesis in Hypernovae is characterized by larger abundance ratios (Zn,Co,V,Ti)/Fe and smaller (Mn,Cr)/Fe than normal SNe, which can explain the observed trends of these ratios in EMP stars. Nucleosynthesis in Faint SNe is characterized by a large amount of fall-back, which explains the abundance pattern of the most Fe-poor stars. These comparisons suggest that black-hole-forming SNe made important contributions to the early Galactic (and cosmic) chemical evolution.

1 Introduction

Massive stars in the range of 8 to $\sim 130M_{\odot}$ undergo core-collapse at the end of their evolution and become Type II and Ib/c supernovae (SNe) unless the entire star collapses into a black hole with no mass ejection (e.g., 5; 37; 28). Here, supernovae are classified based on the maximum light spectra as follows (e.g., 21). Type II supernovae (SNe II) are defined by the presence of hydrogen, which implies that the progenitors are red (or blue) supergiants keeping their hydrogen-rich envelope. Type Ib supernovae (SNe Ib) are characterized by the lack of hydrogen but the presence of prominent He lines, so that their progenitors are Wolf-Rayet (WN) or He stars losing their H-rich envelope in a stellar wind or by Roche lobe overflow in binary systems. Type Ic supernovae (SNe Ic) do not show prominent He lines as well as H, which implies that their progenitors have lost even most of He layers to become WC/WO Wolf-Rayet stars or C+O stars in binary systems (e.g., 78). (In contrast, Type Ia SNe are the thermonuclear explosions of mass accreting white dwarfs in binary systems and spectroscopically characterized by the lack of H and He and the presence of strong Si lines (e.g., 76).)

These supernovae release large explosion energies and eject explosive nucleosynthesis materials, thus having strong dynamical, thermal, and chemical influences on the evolution of interstellar, intergalactic, and intracluster matter (e.g., 29) as well as galaxies and galaxy clusters. Therefore, the explosion energies of core-collapse supernovae are fundamentally important quantities, and an estimate of $E \sim 1 \times 10^{51}$ ergs has often been used in calculating nucleosynthesis and the impact on the interstellar medium. (In the present paper, we use the explosion energy E for the final kinetic energy of explosion, and $E_{51} = E/10^{51}$ erg.) A good example is SN1987A in the Large Magellanic Cloud, whose energy is estimated to be $E_{51} = 1.0 - 1.5$ from its early light curve (e.g., 5; 77).

One of the most interesting recent developments in the study of supernovae is the discovery of some very energetic supernovae, whose kinetic energy (KE) exceeds 10^{52} erg, more than 10 times the KE of normal core-collapse SNe. The most luminous and powerful of these objects, the Type Ic supernova (SN Ic) 1998bw, was linked to the gamma-ray burst GRB 980425 (30), thus establishing for the first time a connection between gamma-ray bursts (GRBs) and the well-studied phenomenon of core-collapse SNe (118; 86; 119). However, SN 1998bw was exceptional for a SN Ic: it was as luminous at peak as a SN Ia, indicating that it synthesized $\sim 0.5M_{\odot}$ of ^{56}Ni , and its KE was estimated at

$$E_{51} \sim 30 \text{ (42)}.$$

In the present paper, we use the term ‘Hypernova (HN)’ to describe such a hyper-energetic supernova with $E \gtrsim 10^{52}$ ergs without specifying the explosion mechanism (80). Following SN 1998bw, other “hypernovae” of Type Ic have been discovered or recognized (82).

Nucleosynthesis features in such hyper-energetic (and hyper-aspherical) supernovae must show some important differences from normal supernova explosions. This might be related to the unpredicted abundance patterns observed in the extremely metal-poor (EMP) halo stars (e.g., 36; 9). This approach leads to identifying the First Stars in the Universe, i.e., metal-free, Population III (Pop III) stars which were born in a primordial hydrogen-helium gas cloud. This is one of the important challenges of the current astronomy (e.g., 116; 1; 12).

More generally, the enrichment by a single SN can dominate the preexisting metal contents in the early universe (e.g., 7; 94; 96; 72). Therefore, the comparison between the SN model and the abundance patterns of EMP stars can provide a new way to find out the individual SN nucleosynthesis.

In §2, we briefly describe how the progenitor mass M and explosion energy E are estimated from the observations of supernovae/hypernovae. In §3, the characteristics of nucleosynthesis in hypernovae are investigated with detailed nucleosynthesis calculations and compared with nucleosynthesis in normal supernovae. In §4, we then discuss possible contribution of hypernovae to the Galactic chemical evolution and on the abundances in metal-poor stars.

2 Hypernovae and Faint Supernovae

The connection between long GRBs and core-collapse SNe has been clearly established from GRB 980425/SN 1998bw (30), GRB 030329/SN 2003dh (99; 38), and GRB 031203/SN 2003lw (62). As summarized in Figure 1, these GRB-SNe have similar properties; they are all hypernovae with $E_{51} \sim 30 - 50$ and synthesize 0.3 - 0.5 M_{\odot} of ^{56}Ni (42; 73; 66).

Hypernovae are also characterized by asphericity from the observations of polarization and emission line features (e.g., 114; 47; 58). The explosion energy of the aspherical models for hypernovae tends to be smaller than the spherical models by a factor of 2 - 3, but still being as high as $E_{51} \gtrsim 10$ (59).

Recently X-Ray Flash (XRF) 060218 has been found to be connected to SN Ic 2006aj (14; 88). Compared with the above GRB-SNe, SN 2006aj is a less

energetic ($E_{51} \sim 2$) SN from a smaller mass progenitor, $\sim 20M_{\odot}$, thus being suggested to be a “neutron star-making SN” (67).

Other non-GRB “hypernovae” have been recognized, such as SN 1997ef (44; 64) and SN 2002ap (65). These hypernovae span a wide range of properties, although they all appear to be highly energetic compared to normal core-collapse SNe. The mass estimates, obtained from fitting the optical light curves and spectra, place hypernovae at the high-mass end of SN progenitors.

In contrast, SNe II 1997D and 1999br were very faint SNe with very low KE (107; 33; 122). In the diagram that shows E and the mass of ^{56}Ni ejected $M(^{56}\text{Ni})$ as a function of the main-sequence mass M_{ms} of the progenitor star (Figure 1), therefore, we propose that SNe from stars with $M_{\text{ms}} \gtrsim 20 - 25M_{\odot}$ have different E and $M(^{56}\text{Ni})$, with a bright, energetic “hypernova branch” at one extreme and a faint, low-energy SN branch at the other (81). For the faint SNe, the explosion energy was so small that most ^{56}Ni fell back onto the compact remnant (e.g., 98). Thus the faint SN branch may become a “failed” SN branch at larger M_{ms} . Between the two branches, there may be a variety of SNe (33; 103).

This trend might be interpreted as follows. Stars more massive than $\sim 25 M_{\odot}$ form a black hole at the end of their evolution. Stars with non-rotating black holes are likely to collapse “quietly” ejecting a small amount of heavy elements (Faint supernovae). In contrast, stars with rotating black holes are likely to give rise to Hypernovae. The hypernova progenitors might form the rapidly rotating cores by spiraling-in of a companion star in a binary system.

3 Nucleosynthesis in Hypernovae

Here we summarize nucleosynthesis yields of core-collapse SN models for 13 – 40 M_{\odot} stars for various explosion energies and progenitor metallicity. Compared with earlier works (120; 102; 79; 93; 16; 56), we focus on (1) Hypernova models to compare with the GRB-SNe and other observations, and (2) Pop III SN models in order to compare with observed abundance patterns of EMP stars.

For HNe, we adopt the ($M_{\text{ms}} - E$) relation as estimated from observations and models of SNe (Fig. 1), i.e., for $M_{\text{ms}} = 20, 25, 30, 40, 50M_{\odot}$, $E_{51} = 10, 10, 20, 30, 40$, respectively. For normal SNe II of 13 - 50 M_{\odot} , $E_{51} = 1$ is assumed (104).

The new ingredients taken into account in the present nucleosynthesis models are: (i) the variation of E (hypernovae, normal SNe, and faint SNe), (ii) the

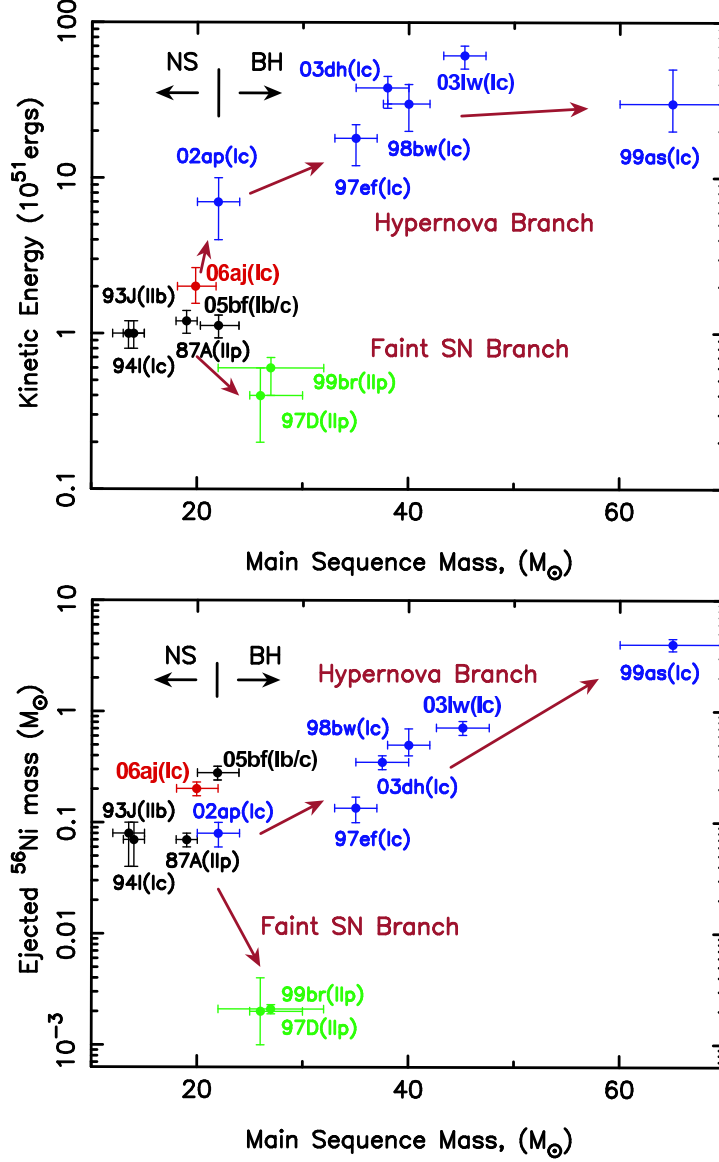


Fig. 1. The explosion energy and the ejected ^{56}Ni mass as a function of the main sequence mass of the progenitors for several supernovae/hypernovae.

mixing and fallback, and (iii) neutrino processes that affects neutron excess near the mass cut.

3.1 Energy Dependence

In core-collapse supernovae/hypernovae, stellar material undergoes shock heating and subsequent explosive nucleosynthesis. Iron-peak elements are produced in two distinct regions, which are characterized by the peak temperature, T_{peak} , of the shocked material. For $T_{\text{peak}} > 5 \times 10^9 \text{K}$, material undergoes complete Si burning whose products include Co, Zn, V, and some Cr after radioactive

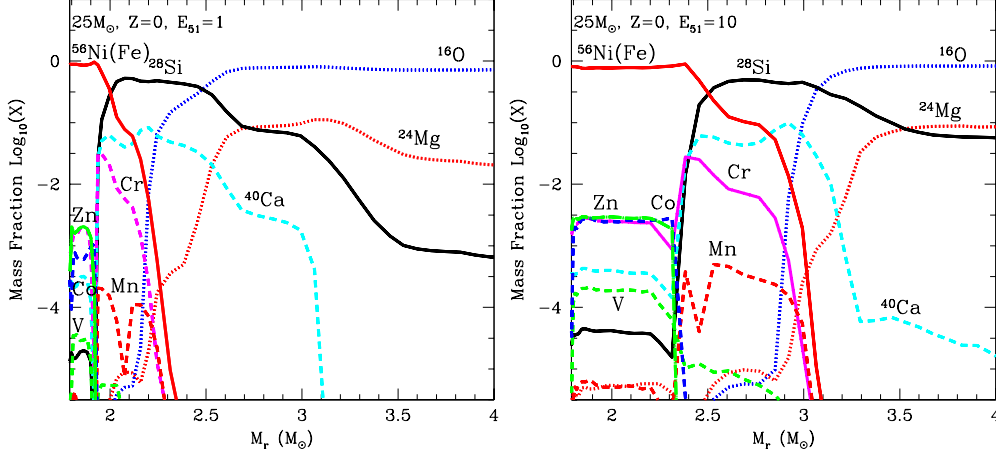


Fig. 2. Abundance distribution against the enclosed mass M_r after the explosion of Pop III $25 M_\odot$ stars with $E_{51} = 1$ (top) and $E_{51} = 10$ (bottom) (109).

decays. For $4 \times 10^9 \text{K} < T_{\text{peak}} < 5 \times 10^9 \text{K}$, incomplete Si burning takes place and its after decay products include Cr and Mn (e.g., 72).

The right panel of Figure 2 shows the composition in the ejecta of a $25 M_\odot$ hypernova model ($E_{51} = 10$). The nucleosynthesis in a normal $25 M_\odot$ SN model ($E_{51} = 1$) is also shown for comparison in the left panel of Figure 2 (109).

We note the following characteristics of nucleosynthesis with very large explosion energies (74; 80; 112):

(i) Both complete and incomplete Si-burning regions shift outward in mass compared with normal supernovae, so that the mass ratio between the complete and incomplete Si-burning regions becomes larger. As a result, higher energy explosions tend to produce larger $[(\text{Zn}, \text{Co}, \text{V})/\text{Fe}]$ and smaller $[(\text{Mn}, \text{Cr})/\text{Fe}]$, which can explain the trend observed in very metal-poor stars (112). (Here $[A/B] = \log_{10}(N_A/N_B) - \log_{10}(N_A/N_B)_\odot$, where the subscript \odot refers to the solar value and N_A and N_B are the abundances of elements A and B, respectively.)

(ii) In the complete Si-burning region of hypernovae, elements produced by α -rich freezeout are enhanced. Hence, elements synthesized through capturing of α -particles, such as ^{44}Ti , ^{48}Cr , and ^{64}Ge (decaying into ^{44}Ca , ^{48}Ti , and ^{64}Zn , respectively) are more abundant.

(iii) Oxygen burning takes place in more extended regions for the larger KE. Then more O, C, Al are burned to produce a larger amount of burning products such as Si, S, and Ar. Therefore, hypernova nucleosynthesis is characterized by large abundance ratios of $[\text{Si}, \text{S}/\text{O}]$, which can explain the abundance feature of M82 (110).

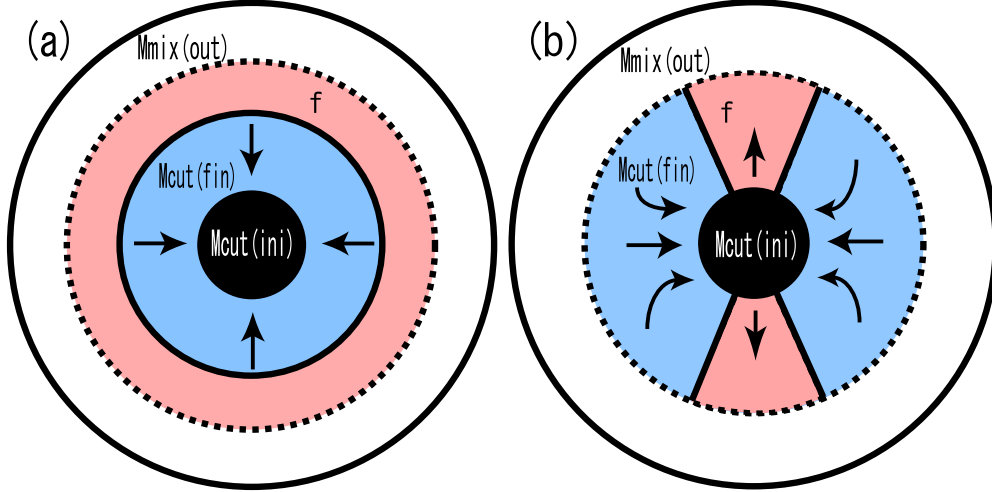


Fig. 3. The illustration of the mixing-fallback model. The central black region is the initial mass cut, that is, inside the inner boundary of the mixing region, $M_{\text{cut}}(\text{ini})$. The mixing region is enclosed with the dotted line at $M_{\text{mix}}(\text{out})$. A fraction f of the materials in the mixing region is ejected into the interstellar space. The rest materials, locating in the gray region inside of $M_{\text{cut}}(\text{fin})$, undergo fallback onto the central remnant. (a) 1-dimensional picture: The materials mixed up to a given radius, and a part of the materials are ejected. (b) 2-dimensional picture: While all materials in the outer region above $M_{\text{mix}}(\text{out})$ are ejected, the materials in the mixing region may be ejected only along the jet-axis. In the jet-like explosion, the ejection factor f depends on the jet-parameters (e.g., an opening angle and an energy injection rate).

3.2 Mixing-Fallback Model

The mixing-fallback models are illustrated in Figures 3ab. First, the inner materials at $M_{\text{cut}}(\text{ini}) \leq M_r \leq M_{\text{mix}}(\text{out})$ are assumed to be mixed by Rayleigh-Taylor instabilities and/or aspherical explosions during the shock wave propagations in the star (e.g., 32; 48). In fact, the post-shock materials are convectively unstable because of deceleration. Later, some fraction of materials in the mixing region undergoes fallback onto the central remnant by gravity (e.g., 120; 45), and the rests at $M_r \geq M_{\text{cut}}(\text{fin})$ are ejected into interstellar space (Fig. 8). The yields are made from the materials which exist above the mixing region and which do not fall back. The degree of fallback depends on the explosion energy, the gravitational potential, and asphericity.

Fallback can take place not only for relatively low energy explosions but also for very energetic jet-like explosions. In fact, Maeda et al. (59) have simulated jet-like explosions and showed that their yields can be similar to the mixing-fallback model because the materials around the jet axis are ejected and the materials around the equatorial plane fallback onto the central remnant. The jet-like explosion is consistent with a recently observed association between

HNe and GRBs with highly collimated relativistic jets. The mixing-fallback model mimics such aspherical explosions, although the spherical model tends to require larger explosion energies than the jet model to obtain similar yields (59).

3.3 Neutron-Proton Ratio near Mass Cut

Recent studies (e.g., 92; 46; 54; 55; 25; 13) have suggested that Y_e may be significantly varied by the neutrino process during explosion. The region, where the neutrino absorption and the Y_e variation occur, is Rayleigh-Taylor unstable, thus having a large uncertainty in Y_e distribution.

In most of present models, following Y_e profile is adopted: $Y_e = 0.5001$ in the complete Si burning region and $Y_e = 0.4997$ in the incomplete Si burning region (112). Lower Y_e in the incomplete Si-burning region leads to larger Mn/Fe, and larger Y_e in the complete Si-burning region leads to even larger Co/Fe.

4 Comparison with the Abundance Patterns of Metal-Poor Stars

Cayrel et al. (15) provided abundance patterns of 35 metal-poor stars with small error bars for $-4.2 \lesssim [\text{Fe}/\text{H}] \lesssim -2.0$. Among the observed abundances, CNO elements might be affected by the deep mixing in the evolved metal-poor stars themselves, which itself is very interesting. On the other hand, the abundance patterns of heavier elements, e.g., Fe-peak elements, must reflect the abundances of interstellar gases out of which the stars were formed, thus providing us with the earliest chemical enrichment in the galaxy. These patterns have provided excellent materials to compare with the SN/HN nucleosynthesis yields.

4.1 Very Metal-Poor (VMP) Stars

VMP stars defined as $[\text{Fe}/\text{H}] \lesssim -2.5$ (9) are likely to have the abundance pattern of well-mixed ejecta of many SNe. We thus compare the abundance patterns of VMP stars with the SN yields integrated over the progenitors of 10 - 50 M_\odot (Fig. 5).

Since the abundance patterns of supernova models with $[\text{Fe}/\text{H}] \lesssim -2.5$ are quite similar to those of Pop III star models (108; 120), we use the Pop III yields for VMP and EMP stars. Comparison between the integrated yields

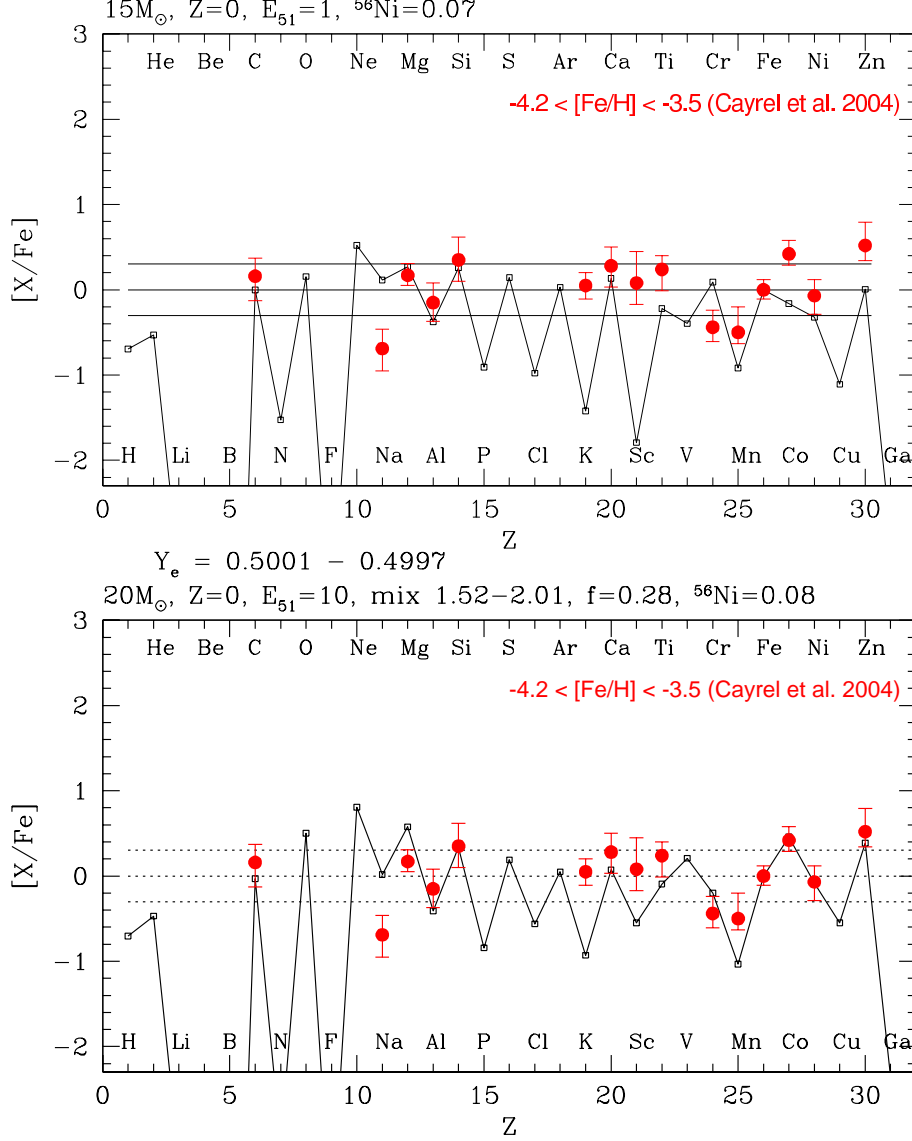


Fig. 4. Averaged elemental abundances of stars with $[Fe/H] = -3.7$ (15) compared with the normal SN yield (upper: $15 M_{\odot}$, $E_{51} = 1$) and the hypernova yield (lower: $20 M_{\odot}$, $E_{51} = 10$).

over the Salpeter's IMF and the abundance pattern of VMP stars (Fig. 5) show that many elements are in reasonable agreements.

Figure 5 shows that N is underproduced in these models. There are two possible explanations for this discrepancy:

(i) N was underproduced in the Pop III SN as in these models, but was enhanced as observed during the first dredge-up in the low-mass red-giant EMP stars (e.g., 117; 100). Actually, most EMP stars are red-giants.

(ii) N was enhanced in massive progenitor stars before the SN explosion. N is

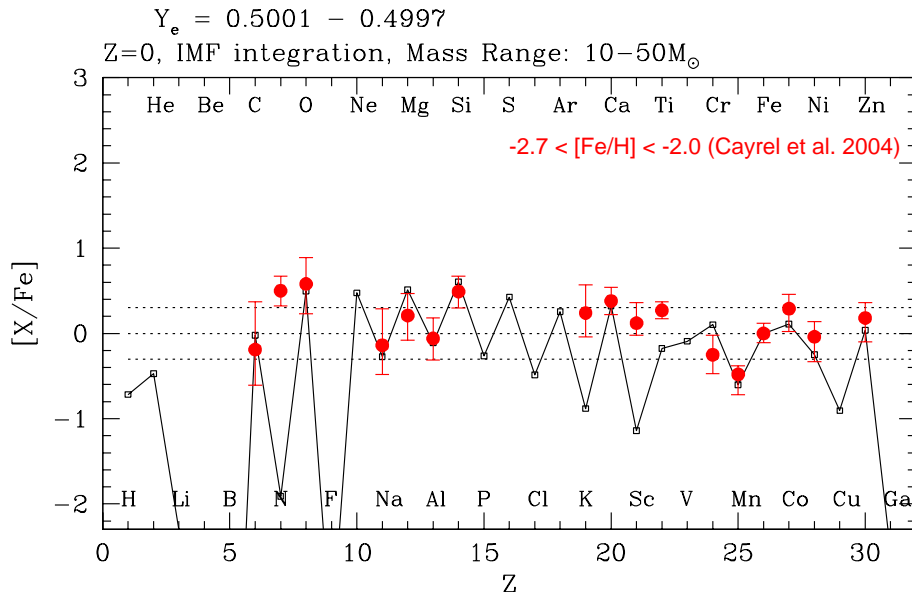


Fig. 5. Comparison between the abundance pattern of VMP stars (15) (*filled circles with error bars*) and the IMF integrated yield of Pop III SNe from $10M_\odot$ to $50M_\odot$ (104)

mainly synthesized by the mixing between the He convective shell and the H-rich envelope (e.g., 108; 45). Mixing can be enhanced by rotation (53; 34; 61). Suppose that the Pop III SN progenitors were rotating faster than more massive stars because of smaller mass loss, then $[N/Fe]$ was enhanced as observed in EMP stars.

4.2 Extremely Metal-Poor (EMP) Stars

In the early galactic epoch when the galaxy was not yet chemically well-mixed, each EMP star may be formed mainly from the ejecta of a single Pop III SN (although some of them might be the second or later generation SNe) (e.g., 4; 105). The formation of EMP stars was driven by a supernova shock, so that $[Fe/H]$ was determined by the ejected Fe mass and the amount of circumstellar hydrogen swept-up by the shock wave (94). Then, hypernovae with larger E are likely to induce the formation of stars with smaller $[Fe/H]$, because the mass of interstellar hydrogen swept up by a hypernova is roughly proportional to E (94; 96) and the ratio of the ejected iron mass to E is smaller for hypernovae than for normal supernovae.

The theoretical yields are compared with the averaged abundance pattern of four EMP stars, CS 22189-009, CD-38:245, CS 22172-002 and CS 22885-096, which have low metallicity ($-4.2 < [Fe/H] < -3.5$) and normal $[C/Fe] \sim 0$ (15).

Figure 4 shows that the averaged abundances of EMP stars can be fitted well with the hypernova model of $20 M_{\odot}$ and $E_{51} = 10$ (lower) but not with the normal SN model of $15 M_{\odot}$ and $E_{51} = 1$ (upper) (83; 104).

In the normal SN model (upper), the mass-cut is determined to eject Fe of mass $0.14 M_{\odot}$. Then the yields are in reasonable agreements with the observations for $[(\text{Na}, \text{Mg}, \text{Si})/\text{Fe}]$, but give too small $[(\text{Mn}, \text{Co}, \text{Ni}, \text{Zn})/\text{Fe}]$ and too large $[(\text{Ca}, \text{Cr})/\text{Fe}]$.

In the HN model (lower), these ratios are in much better agreement with observations. The ratios of Co/Fe and Zn/Fe are larger in higher energy explosions since both Co and Zn are synthesized in complete Si burning at high temperature region (see the next subsection). To account for the observations, materials synthesized in a deeper complete Si-burning region should be ejected, but the amount of Fe should be small. This is realized in the mixing-fallback models (109; 112).

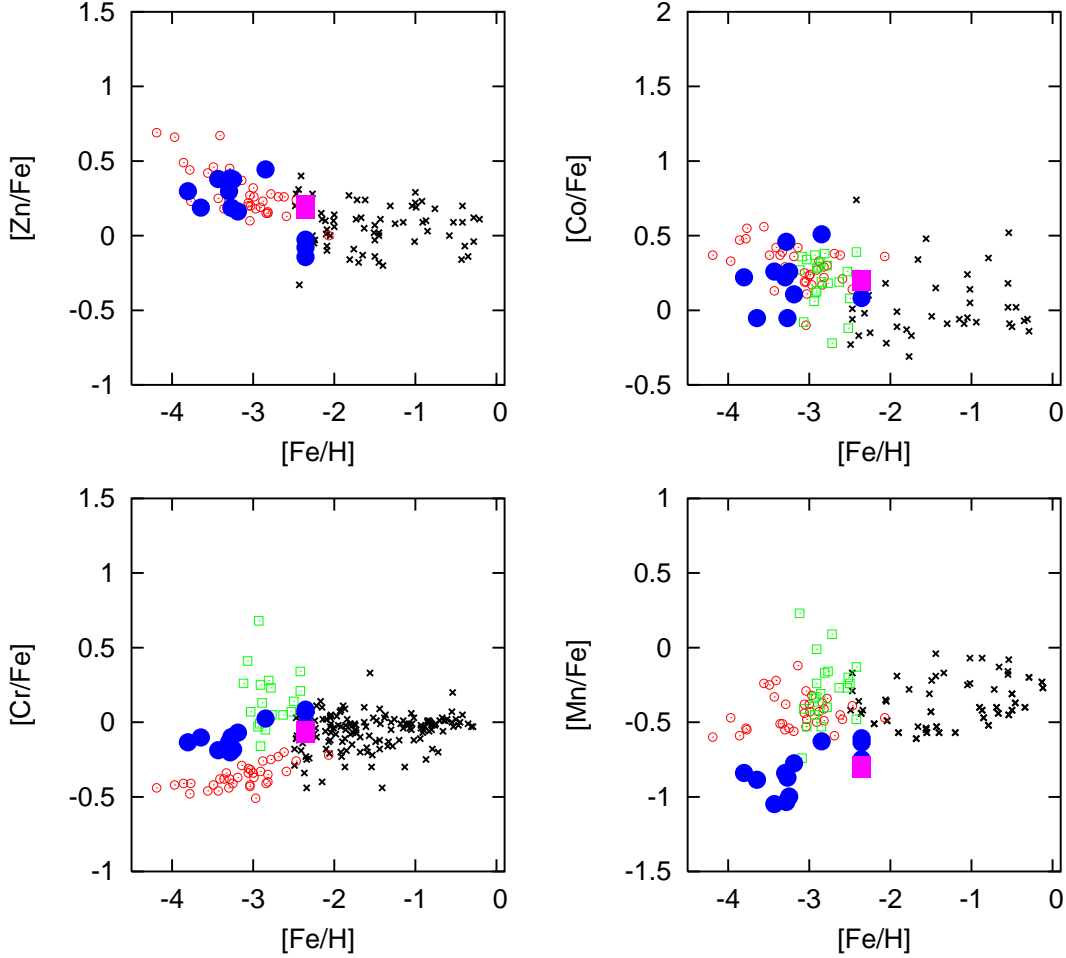


Fig. 6. Observed abundance ratios of $[\text{Zn}, \text{Co}, \text{Cr}, \text{Mn}/\text{Fe}]$ vs $[\text{Fe}/\text{H}]$ [*open circle*: (15); *open square*: (39)] compared with individual Pop III SN models (*filled circle*) and IMF-integrated models (*filled square*).

4.3 Hypernovae and Fe-peak Elements (Cr, Mn, Fe, Zn, Co, Zn)

In the observed abundances of halo stars, there are significant differences between the abundance patterns in the iron-peak elements below and above $[\text{Fe}/\text{H}] \sim -2.5$ - -3 .

(i) For $[\text{Fe}/\text{H}] \lesssim -2.5$, the mean values of $[\text{Cr}/\text{Fe}]$ and $[\text{Mn}/\text{Fe}]$ decrease toward smaller metallicity, while $[\text{Co}/\text{Fe}]$ increases (68; 94). [The negligibly weak trend in $[\text{Mn}/\text{Fe}]$ in (15) is different from previous observations that $[\text{Mn}/\text{Fe}]$ decreases significantly for smaller $[\text{Fe}/\text{H}]$ (68).]

(ii) $[\text{Zn}/\text{Fe}] \sim 0$ for $[\text{Fe}/\text{H}] \simeq -3$ to 0 (97), while at $[\text{Fe}/\text{H}] < -3.3$, $[\text{Zn}/\text{Fe}]$ increases toward smaller metallicity (15).

The larger $[(\text{Zn}, \text{Co})/\text{Fe}]$ and smaller $[(\text{Mn}, \text{Cr})/\text{Fe}]$ in the supernova ejecta can be realized if the mass ratio between the complete Si burning region and the incomplete Si burning region is larger, or equivalently if deep material from the complete Si-burning region is ejected by mixing or aspherical effects. This can be realized if (i) the mass cut between the ejecta and the compact remnant is located at smaller M_r (72), (ii) E is larger to move the outer edge of the complete Si burning region to larger M_r (74), or (iii) asphericity in the explosion is larger.

Among these possibilities, a large explosion energy E enhances α -rich freeze-out, which results in the increase of the local mass fractions of Zn and Co, while Cr and Mn are not enhanced (109). Models with $E_{51} = 1$ do not produce sufficiently large $[\text{Zn}/\text{Fe}]$. To be compatible with the observations of $[\text{Zn}/\text{Fe}] \sim 0.5$, the explosion energy must be much larger, i.e., $E_{51} \gtrsim 20$ for $M \gtrsim 20M_\odot$, i.e., hypernova-like explosions of massive stars ($M \gtrsim 25M_\odot$) with $E_{51} > 10$ are responsible for the production of Zn.

Figure 2 exhibits that the high-energy models tend to be located at lower $[\text{Fe}/\text{H}]$ in the SN-induced star formation scenario. Here we use the HN models with $E_{51} = 10, 10, 20, 30, 40$ for $M_{\text{ms}} = 20, 25, 30, 40, 50M_\odot$, respectively. In this scenario, EMP stars are enriched by a single supernova (7) which ejects Fe of mass $M(\text{Fe})$ and the hydrogen mass swept by supernova ejecta is proportional to the explosion energy. Then this model gives:

$$[\text{Fe}/\text{H}] = \log_{10}(M(\text{Fe})/E_{51}) - \text{const.} \quad (1)$$

$[\text{Ni}/\text{Fe}]$ and $[\text{Zn}/\text{Fe}]$ in our models are in good agreements with the observations, although $[\text{Ni}/\text{Fe}]$ is slightly smaller than the observation. Ni/Fe is larger if $M_{\text{cut}}(\text{ini})$ is smaller (i.e., the mass cut is deeper) because ^{58}Ni , a main isotope

of Ni, is mainly synthesized in a deep region with $Y_e < 0.5$. However, a smaller $M_{\text{cut}}(\text{ini})$ tends to suppress Zn/Fe thus requiring more energetic explosions.

The good agreement of [Zn/Fe] strongly support the SN-induced star formation model and suggest that EMP stars with lower [Fe/H] might be made from the ejecta of HNe with larger explosion energies and larger progenitor's masses. See, however, (22).

If VMP stars with [Fe/H] ~ -2.5 is made from normal SNe with $E_{51} = 1$, Zn is underproduced in our models. 1D nucleosynthesis studies with neutrino transport (25; 26; 90) suggested that Zn in the normal SN model is enhanced to [Zn/Fe] ~ 0 as well as the enhancement of [Sc/Fe]. However, the enhancement is not large enough to explain the high [Zn/Fe] ($\gtrsim 0.5$) in the EMP stars.

Figure 2 shows that [Cr/Fe] in our models is larger than (15), although the trend in our models is similar to the observations. Since Cr is mostly produced in the incomplete Si-burning region, the relative size of the region should be smaller than the present model in order to produce smaller Cr/Fe.

[Mn/Fe] and [Co/Fe] in our models are smaller than the observations, although the trend of [Co/Fe] in our models is similar to the observations. Mn can be efficiently enhanced by lowering Y_e (112) and by a neutrino process (120). Therefore the Mn/Fe ratio is important to constrain the physical processes during the explosion.

4.4 Carbon-Rich Extremely Metal-Poor Stars

Stars with large [C/Fe] (~ 1), called C-rich EMP stars, are discussed in (111; 112). The origin of those stars may be different from those of [C/Fe] ~ 0 stars. The large [C/Fe] ($\gtrsim 0.5$) can be understood as the faint SN origin, because the faint SNe are characterized by a large amount of Fe fallback that leads to large [(C, N, O)/Fe] (111; 112). Figure 7 shows the comparison between the abundance pattern of C-rich EMP stars (CS 29498-043: (2)) and the $25 M_{\odot}$ faint SN model (104).

Most C-rich EMP stars show O/Mg being significantly larger than the solar ratio. Faint SNe enhance [O/Fe] more effectively than [Mg/Fe], because Mg is synthesized in the inner region and thus fallen-back onto the central remnant more preferentially than O. (Note that the abundance determination of O is subject to the uncertain hydrodynamical (3D) effects (75).)

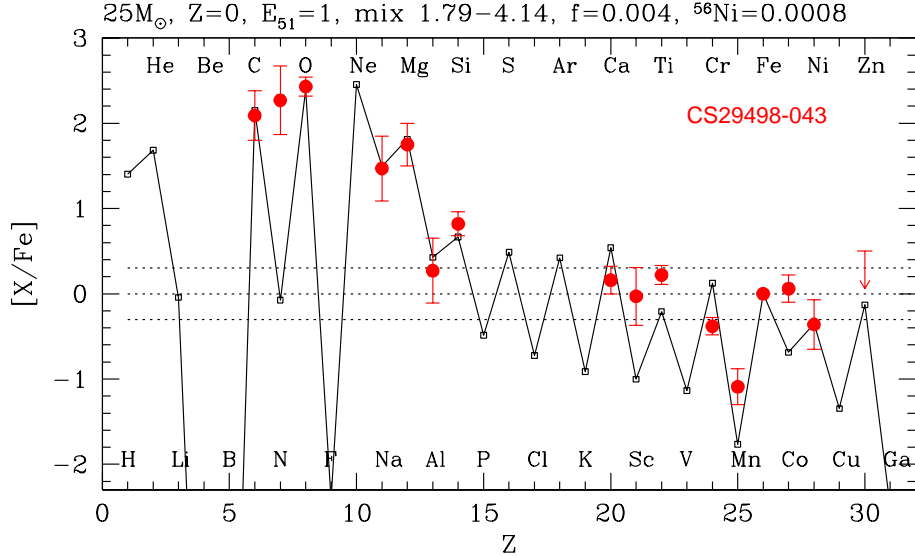


Fig. 7. Comparison between the abundance pattern of the C-rich EMP star (CS 29498-043: *filled circles with error bars* (2)) and the theoretical yields of the $25 M_{\odot}$ faint SN (*solid line* (104)).

5 Hyper Metal-Poor (HMP) Stars

5.1 HE0107-5240 & HE1327-2326

Recently two hyper metal-poor (HMP) stars, HE0107-5240 (17) and HE1327-2326 (23), were discovered, whose metallicity Fe/H is smaller than $1/100,000$ of the Sun (i.e., $[\text{Fe}/\text{H}] < -5$), being more than a factor of 10 smaller than previously known extremely metal-poor (EMP) stars. These discoveries have raised an important question as to whether the observed low mass ($\sim 0.8 M_{\odot}$) HMP stars are actually Pop III stars (117; 100), or whether these HMP stars are the second generation stars being formed from gases which were chemically enriched by a single first generation supernova (SN) (111; 57). This is related to the questions of how the initial mass function depends on the metallicity (e.g., 95). Thus identifying the origin of these HMP stars is indispensable to the understanding of the earliest star formation and chemical enrichment history of the Universe.

The elemental abundance patterns of these HMP stars provide a key to the answer to the above questions. The abundance patterns of HE1327-2326 (23; 3; 24) and HE0107-5240 (18; 11; 18) are quite unusual (Fig. 8). The striking similarity of $[\text{Fe}/\text{H}]$ ($= -5.4$ and -5.2 for HE1327-2326 and HE0107-5240, respectively) and $[\text{C}/\text{Fe}]$ ($\sim +4$) suggests that similar chemical enrichment mechanisms operated in forming these HMP stars. However, the N/C and $(\text{Na}, \text{Mg}, \text{Al})/\text{Fe}$ ratios are more than a factor of 10 larger in HE1327-2326. In order for the theoretical models to be viable, these similarities and differences

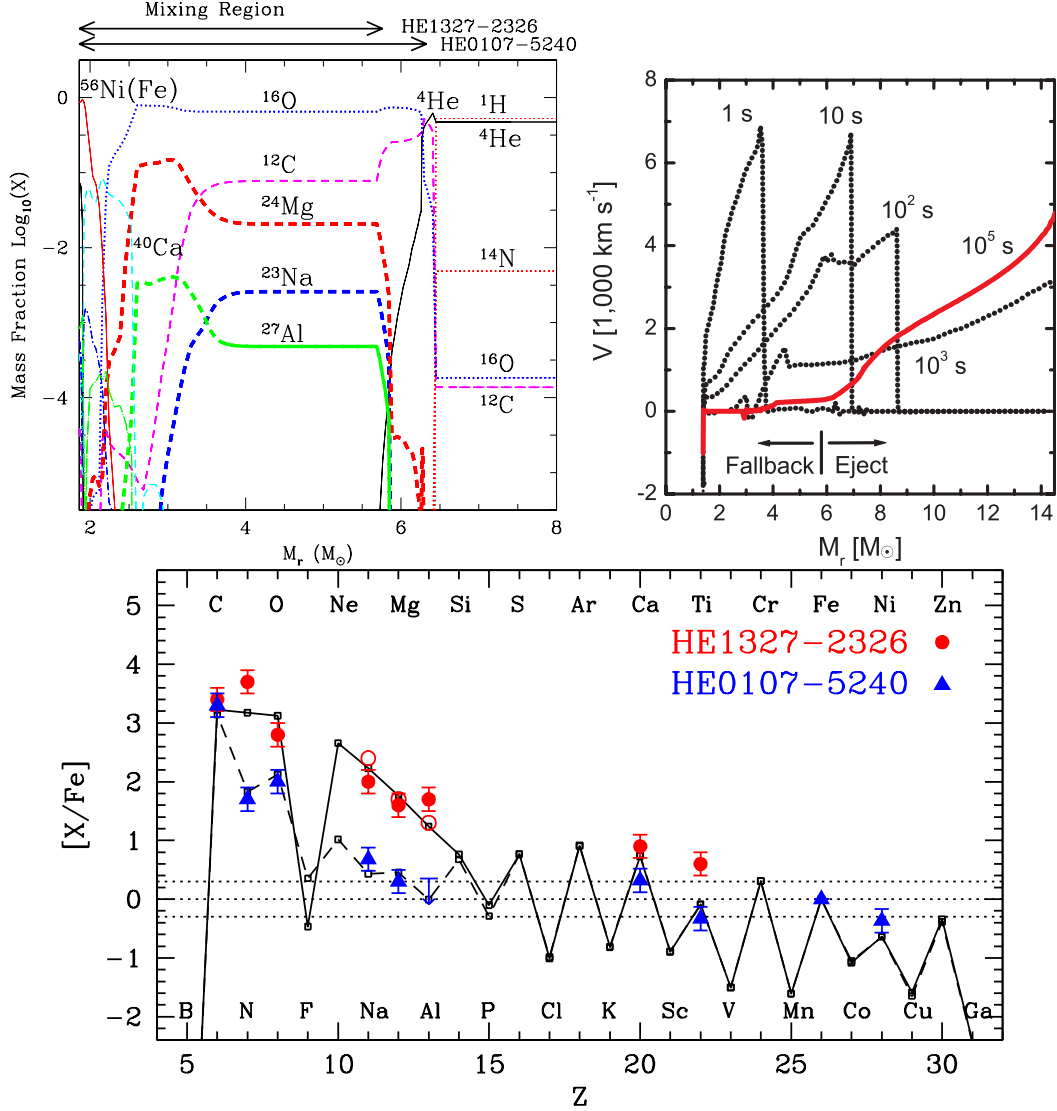


Fig. 8. (upper-left): The post-explosion abundance distributions for the $25 M_{\odot}$ model with the explosion energy $E_{51} \sim 0.7$ (45). (upper-right): Propagation of the shock wave and fallback for the HE1327-2326 model (45). (lower): Elemental abundances of the C-rich HMP stars HE0107-5240 (filled triangles: 18; 19) and HE1327-2326 (filled circles: 23; 24) compared with theoretical supernova yields.

should be explained self-consistently.

Iwamoto et al. (45) showed that the above similarities and variations of the HMP stars can be well reproduced in unified manner by nucleosynthesis in the core-collapse “faint” supernovae (SNe) which undergo mixing-and-fallback (111). We thus argue that the HMP stars are the second generation low mass stars, whose formation was induced by the first generation (Pop III) SN with efficient cooling of carbon-enriched gases.

5.2 Models for Hyper Metal-Poor Stars

We consider a model that C-rich EMP stars are produced in the ejecta of (almost) metal-free supernova mixed with extremely metal-poor interstellar matter. The similarity of $[\text{Fe}/\text{H}]$ and $[\text{C}/\text{Fe}]$ suggests that the progenitor’s masses of Pop III SNe were similar for these HMP stars. We therefore choose the Pop III 25 M_{\odot} models and calculate their evolution and explosion (111; 45).

The abundance distribution after explosive nucleosynthesis is shown in Figure 8 (upper-left) for the kinetic energy E of the ejecta $E_{51} \equiv E/10^{51}$ erg = 0.74. The abundance distribution for $E_{51} = 0.71$ is similar. In the “faint” SN model, most part of materials that underwent explosive nucleosynthesis are decelerated by the influence of the gravitational pull (120) and will eventually fall back onto the central compact object. The explosion energies of $E_{51} = 0.74$ and 0.71 lead to the mass cut $M_{\text{cut}} = 5.8M_{\odot}$ and $6.3M_{\odot}$, respectively (Fig.8: upper-right), and the former and the latter models are used to explain the abundance patterns of HE1327–2326 and HE0107–5240, respectively.

During the explosion, the SN ejecta is assumed to undergo mixing, i.e., materials are first uniformly mixed in the mixing-region extending from $M_r = 1.9M_{\odot}$ to the mass cut at $M_r = M_{\text{cut}}$ (where M_r is the mass coordinate and stands for the mass interior to the radius r) as indicated in Figure 8 (left), and only a tiny fraction, f , of the mixed material is ejected from the mixing-region together with all materials at $M_r > M_{\text{cut}}$; most materials interior to the mass cut fall back onto the central compact object. Such a mixing-fallback mechanism (which might mimic a jet-like explosion) is required to extract Fe-peak and other heavy elements from the deep fallback region into the ejecta (111; 112).

Figure 8 (lower) shows the calculated abundance ratios in the SN ejecta models for suitable choice of f which are respectively compared with the observed abundances of the two HMP stars. To reproduce $[\text{C}/\text{Fe}] \sim +4$ and other abundance ratios of HMP stars in Figure 8 (lower), the ejected mass of Fe is only $1.0 \times 10^{-5}M_{\odot}$ for HE1327–2326 and $1.4 \times 10^{-5}M_{\odot}$ for HE0107–5240. These SNe are much fainter in the radioactive tail than the typical SNe and form massive black holes of $\sim 6M_{\odot}$.

The question is what causes the large difference in the amount of Na-Mg-Al between the SNe that produced HE0107–5240 and HE1327–2326. Because very little Na-Mg-Al is ejected from the mixed fallback materials (i.e., $f \sim 10^{-4}$) compared with the materials exterior to the final mass cut $M_{\text{cut}}(\text{fin})$, the ejected amount of Na-Mg-Al is very sensitive to the location of the mass cut. As indicated in Figure 8, $M_{\text{cut}}(\text{fin})$ is smaller (i.e., the fallback mass is smaller) in the model for HE1327–2326 ($M_{\text{cut}}(\text{fin}) = 5.8M_{\odot}$) than HE0107–

5240 ($M_{\text{cut}}(\text{fin}) = 6.3M_{\odot}$), so that a larger amount of Na-Mg-Al is ejected from the SN for HE1327–2326. Since $M_{\text{cut}}(\text{fin})$ is sensitively determined by the explosion energy, the (Na-Mg-Al)/Fe ratios among the HMP stars are predicted to show significant variations and can be used to constrain E_{51} . Note also that the explosion energies of these SN models with fallback are not necessarily very small (i.e., $E_{51} \sim 0.7$). Further these explosion energies are consistent with those observed in the actual “faint” SNe (107).

The next question is why HE1327–2326 has a much larger N/C ratio than HE0107–5240. In our models, a significant amount of N is produced by the mixing between the He convective shell and the H-rich envelope during the presupernova evolution (108), where C created by the triple- α reaction is burnt into N through the CN cycle. For the HE1327–2326 model, we assume about 30 times larger diffusion coefficients (i.e., faster mixing) for the H and He convective shells to overcome an inhibiting effect of the mean molecular weight gradient (and also entropy gradient) between H and He layers. Thus, larger amounts of protons are carried into the He convective shell. Then $[C/N] \sim 0$ is realized as observed in HE1327–2326. Such an enhancement of mixing efficiency has been suggested to take place in the present-day massive stars known as fast rotators, which show various N and He enrichments due to different rotation velocities (34; 70).

Recent works have taken into account the NLTE effects and 3D effects, and obtained $[O/Fe]$ (24; 19). The resultant abundance patterns are shown in Figure 8 (lower) and the newly obtained $[O/Fe]$ in HE1327–2326 is consistent with our theoretical models.

6 Nucleosynthesis in Aspherical Supernovae

If supernova explosions are not spherically symmetric, resultant nucleosynthesis is somewhat different from spherical explosions. Here we discuss nucleosynthesis in bipolar (jet-like) explosions (71; 58; 59; 60).

In the jet-like explosion model, the shock wave is stronger along the z -axis and heats up the stellar material to higher temperatures. Along the r -axis, temperatures are lower because of the weaker shock and densities are higher because of mass accretion. Therefore, the materials along the z -axis occupy the high entropy region in the $\rho - T$ plane, while those in the r -axis form the lowest bound of entropy. As a result, ^{56}Ni is synthesized preferentially along the z -axis, while a lot of unburned materials, mainly O, are left at low velocity in the r -plane.

Because the bipolar models preferentially eject the materials experiencing

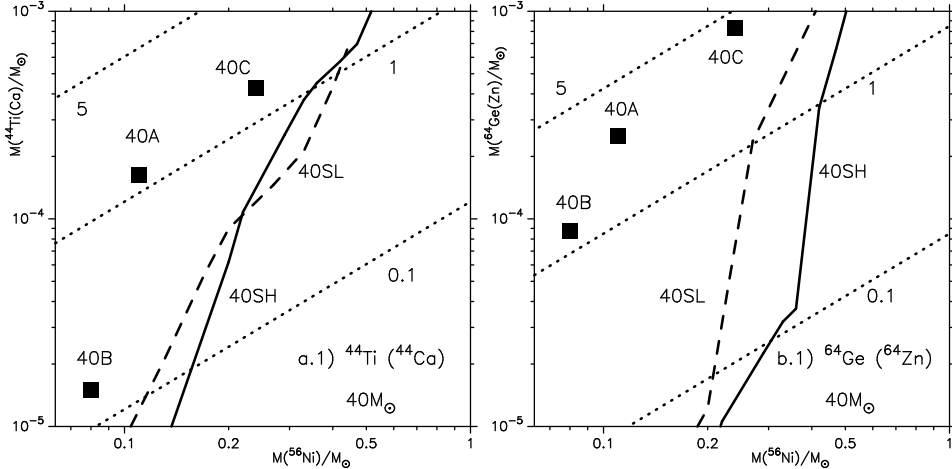


Fig. 9. Ejected masses of ^{44}Ti (left) and ^{64}Ge (right) as a function of $M(^{56}\text{Ni})$ for some bipolar models (40A, B, and C: filled squares) and for spherical models (40SH, SL: lines). The dotted lines show the ratio $(^{44}\text{Ca}, ^{64}\text{Zn})/^{56}\text{Fe}$ relative to the solar value (59).

higher temperatures (higher entropies) in complete silicon burning, the ratios $^{44}\text{Ti}/^{56}\text{Ni}$ and $^{64}\text{Ge}/^{56}\text{Ni}$ are significantly larger in the bipolar models than spherical models. Such an enhancement of the α -rich freezeout products is seen in Figure 9. For a given mass of ^{56}Ni , the aspherical models (denoted as 40A, B, C) eject larger amount of ^{44}Ti and ^{64}Zn . Such enhancement could be important to solve problems related to the production of ^{44}Ti (101).

As a result, the aspherical models produce the overall abundance patterns being different from spherical models (Fig. 10). $[(\text{Zn}, \text{Co})/\text{Fe}]$ are enhanced, while $[(\text{Mn}, \text{Cr})/\text{Fe}]$ are suppressed. These trends are similar to ones observed in EMP stars (68), thus suggesting important roles of hypernovae in the early Galactic chemical evolution.

7 The First Stars

It is of vital importance to identify the first generation stars in the Universe, i.e., totally metal-free, Pop III stars. The impact of the formation of Pop III stars on the evolution of the Universe depends on their typical masses.

7.1 High Mass vs. Low Mass

Recent numerical models have shown that, the first stars are as massive as $\gtrsim 100 M_{\odot}$ (1; 12) (VMS: very massive stars). The formation of long-lived low

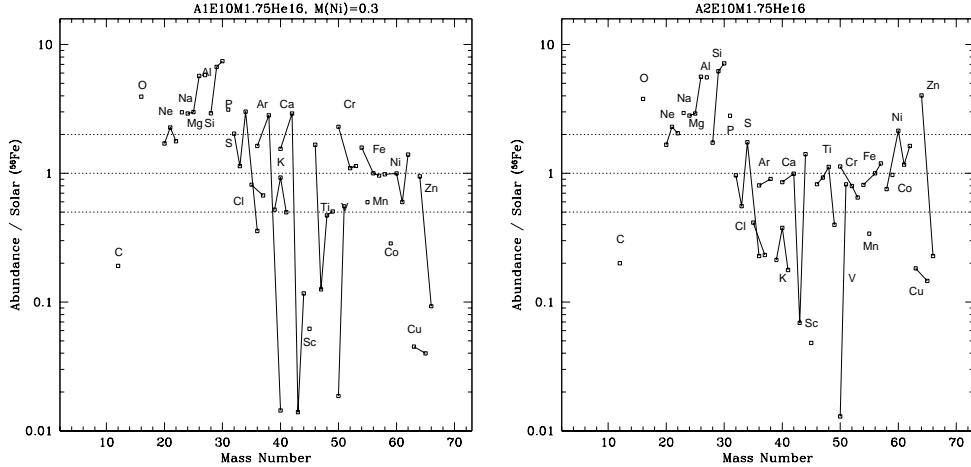


Fig. 10. Isotopic yields of spherical (left) and aspherical (right) explosions (60). In both cases, the progenitor is the $16M_{\odot}$ He core of the $40M_{\odot}$ star, and the explosion energy is $E_{51} \equiv E/10^{51}$ erg = 10. The mass of ^{56}Ni is $0.3M_{\odot}$ (spherical) and $0.24M_{\odot}$ (aspherical), and these values give $[\text{O}/\text{Fe}] \sim 0.5$ being consistent with observed in extremely metal poor stars.

Table 1

Stabilities of Pop III and Pop I massive stars: \bigcirc and \times indicate that the star is stable and unstable, respectively. The e -folding time for the fundamental mode is shown after \times in units of 10^4yr (81).

$M(M_{\odot})$	80	100	120	150	180	300
Pop III	\bigcirc	\bigcirc	\bigcirc	\times (9.03)	\times (4.83)	\times (2.15)
Pop I	\bigcirc	\times (7.02)	\times (2.35)	\times (1.43)	\times (1.21)	\times (1.71)

mass Pop III stars may be inefficient because of slow cooling of metal free gas cloud, which is consistent with the failure of attempts to find Pop III stars.

If the HMP stars are Pop III low mass stars that has gained its metal from a companion star or interstellar matter (121), would it mean that the above theoretical arguments are incorrect and that such low mass Pop III stars have not been discovered only because of the difficulty in the observations?

Based on the results in the earlier section, we propose that the first generation supernovae were the explosion of $\sim 20\text{-}130 M_{\odot}$ stars and some of them produced C-rich, Fe-poor ejecta. Then the low mass star with even $[\text{Fe}/\text{H}] < -5$ can form from the gases of mixture of such a supernova ejecta and the (almost) metal-free interstellar matter, because the gases can be efficiently cooled by enhanced C and O ($[\text{C}/\text{H}] \sim -1$).

7.2 Pair Instability SNe vs. Core Collapse SNe

In contrast to the core-collapse supernovae of 20-130 M_{\odot} stars, the observed abundance patterns cannot be explained by the explosions of more massive, 130 - 300 M_{\odot} stars. These stars undergo pair-instability supernovae (PISNe) and are disrupted completely (e.g., 109; 35), which cannot be consistent with the large C/Fe observed in HMP stars and other C-rich EMP stars. The abundance ratios of iron-peak elements ($[\text{Zn}/\text{Fe}] < -0.8$ and $[\text{Co}/\text{Fe}] < -0.2$) in the PISN ejecta (Fig. 4; (109; 35)), cannot explain the large Zn/Fe and Co/Fe in the typical EMP stars (68; 84; 15) and CS22949-037 either. Therefore the supernova progenitors that are responsible for the formation of EMP stars are most likely in the range of $M \sim 20 - 130 M_{\odot}$, but not more massive than 130 M_{\odot} (also 106). This upper limit mass of the Zero Age Main Sequence (ZAMS) star depends on the stability of massive stars.

To determine the above upper limit mass, non-adiabatic stabilities of massive ($80M_{\odot} - 300M_{\odot}$) Pop III stars have been analyzed using a radial pulsation code following (40; 8; 81). Because CNO elements are absent during the early stage of their evolution, the CNO cycle does not operate and the star contracts until temperature rises sufficiently high for the 3α reaction to produce ^{12}C . These stars were found to have $X_{\text{CNO}} \sim 1.6 - 4.0 \times 10^{-10}$, and the central temperature $T_c \sim 1.4 \times 10^8$ K on their ZAMS.

As summarized in Table 1 (81), the critical mass of ZAMS Pop III star is $128M_{\odot}$ while that of Pop I star is $94M_{\odot}$. This difference comes from very compact structures (with high T_c) of Pop III stars. Stars more massive than the critical mass will undergo pulsation and mass loss. We note that the e -folding time of instability is much longer for Pop III stars than Pop I stars with the same mass, and thus the mass loss rate is much lower. These results are consistent with (40; 8). The absence of the indication of PISNe in EMP stars might imply that these massive stars above $130M_{\odot}$ undergo significant mass loss, thus evolving into Fe core-collapse rather than PISNe.

Alternative possibility is that the First Stars were even more massive than $\sim 300M_{\odot}$ (115; 91; 27; 85). Such massive stars undergo core-collapse (CVMS: core-collapse VMS) to form Intermediate mass black holes. If such stars formed rapidly rotating black holes, jet-like mass ejection could produce interesting nucleosynthesis materials to compare with the elemental abundances observed in the ICM, IGM, and M82 (85).

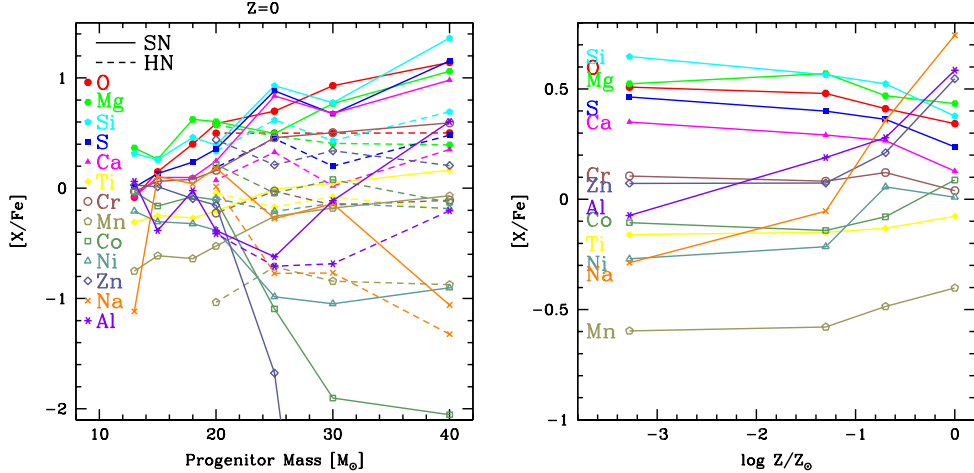


Fig. 11. (left:) Relative abundance ratios as a function of progenitor mass with $Z = 0$. The solid and dashed lines show normal SNe II with $E_{51} = 1$ and HNe. (right:) The IMF weighted abundance ratios as a function of metallicity of progenitors, where the HN fraction $\epsilon_{\text{HN}} = 0.5$ is adopted. Results for $Z = 0$ are plotted at $\log Z/Z_{\odot} = -4$.

8 Galactic Chemical Evolution

8.1 Nucleosynthesis and Metallicity

We have calculated the chemical yields for various metallicities, including Hypernovae (104) as described earlier. For this set of yields calculations, we assume $Y_e = 0.4997$ in incomplete Si-burning region, but use the original Y_e (112) (rather than $Y_e = 0.5001$) in the complete Si-burning region.

Table 2 gives the resultant nucleosynthesis yields in units of solar mass for SNe II and HNe as functions of the progenitor mass ($M = 13, 15, 18, 20, 25, 30, 40 M_{\odot}$) and metallicity ($Z = 0, 0.001, 0.004, 0.02$). Table 3 gives the IMF weighted yields as a function of metallicity normalized by the total amount of gases forming stars as follows:

$$X(A) = \frac{\int_{0.07M_{\odot}}^{50M_{\odot}} X_M(A) M_{\text{ej}}(M) M^{-2.35} dM}{\int_{0.07M_{\odot}}^{50M_{\odot}} M \times M^{-2.35} dM} \quad (2)$$

where $X(A)$ is an integrated mass fraction of an element, A, $X_M(A)$ is mass fraction of A in a model whose mass is nearest to M , and $M_{\text{ej}}(M)$ is an ejected mass interpolated between the nearest models or the nearest model and the edge of the IMF integrated mass range. Here we assume $M \leq 10M_{\odot}$ and $50M_{\odot}$ stars do not produce materials as Type II SNe or HNe, i.e., $M_{\text{ej}}(M \leq 10M_{\odot}) = M_{\text{ej}}(50M_{\odot}) = 0$.

For HNe, we set $E_{51} = 10, 10, 20,$ and 30 for $20, 25, 30,$ and $40M_{\odot}$, respectively. Although Fe production is larger for more massive stars because of the higher energy, $[\alpha/\text{Fe}]$ is almost constant independent of the stellar mass because we assume the mass-cut to get $[\text{O}/\text{Fe}] = 0.5$. In this set, the abundance ratios of iron-peak elements (Cr, Mn, Co, and Ni) are almost constant because the mixing-fallback parameters are chosen to give the largest $[\text{Zn}/\text{Fe}]$.

Figure 11 shows the abundance ratios of Pop III ($Z = 0$) SNe II and HNe as a function of the progenitor mass (left) and the IMF weighted yields of SNe II and HNe as a function of metallicity (right). The solid and dashed lines show the SN II and HN yields, respectively.

The yield masses of α elements (O, Ne, Mg, Si, S, Ar, Ca, and Ti) are larger for more massive stars because of the larger mantle mass. Since the Fe mass is $\sim 0.1M_{\odot}$, being independent of the progenitor's mass for $E_{51} = 1$, the abundance ratio $[\alpha/\text{Fe}]$ is larger for more massive stars.

In the metal-free stellar evolution, because of the lack of initial CNO elements, the CNO cycle does not operate until the star contracts to a much higher central temperature ($\sim 10^8$ K) than population II stars, where the 3α reaction produces a tiny fraction of ^{12}C ($\sim 10^{-10}$ in mass fraction).

However, the late core evolution and the resulting Fe core masses of metal-free stars are not significantly different from metal-rich stars. Therefore, $[\alpha/\text{Fe}]$ is larger by only a factor of ~ 0.2 dex and the abundance ratios of the iron-peak elements are not so different from metal-rich stars, except for Mn.

On the other hand, the CNO cycle produces only a small amount of ^{14}N , which is transformed into ^{22}Ne during He-burning. The surplus of neutrons in ^{22}Ne increases the abundances of odd-Z elements (Na, Al, P, ...). As a result, the abundances of odd-Z elements depend on the metallicity. $[\text{Na}/\text{Fe}]$ and $[\text{Al}/\text{Fe}]$ of metal-free stars are smaller by ~ 1.0 and 0.7 dex than solar abundance stars, which are consistent with the observed trends.

8.2 Chemical Evolution of the Solar Neighborhood

In the chemical evolution model, we should introduce one important parameter to describe the fraction of hypernovae, ϵ_{HN} . Although the mass-energy relation has been obtained from the light curve modeling for individual supernovae, there is no clear constraint on the energy distribution function because of the poor statistics. ϵ_{HN} may depend on metallicity, and may be constrained with the GRB rate. Here we adopt $\epsilon_{\text{HN}} = 0.5$ independent of the mass and metallicity to find that this provides a good agreement of $[\alpha/\text{Fe}]$ plateau against $[\text{Fe}/\text{H}]$ with observations. We should note that the plateau value depends on

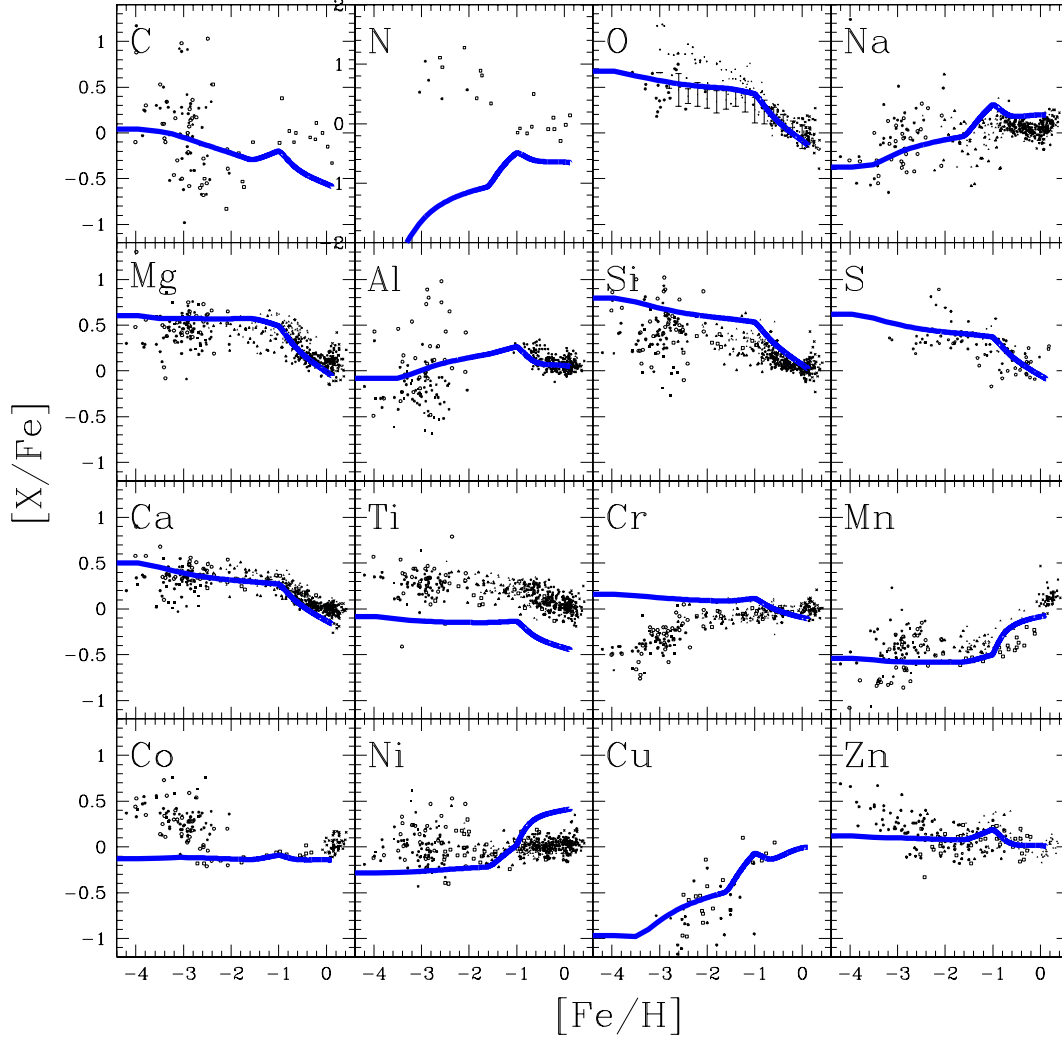


Fig. 12. $[X/Fe]$ - $[Fe/H]$ relations for the model with our yields (solid line) compared with observational data(10; 15; 20; 31; 39; 68; 69; 94).

the IMF, specifically on the slope x and the upper limit M_u .

We use the chemical evolution model that allows the infall of material from outside the disk region (50). We adopt the Galactic age 13 Gyr, infall timescale 5 Gyr, star formation coefficient 0.45 Gyr^{-1} , and the Salpeter IMF with a slope of $x = 1.35$ in the range of $0.07 M_\odot \leq M \leq 50 M_\odot$. The treatment of SNe Ia is the same as in (50) but with $[b_{\text{RG}} = 0.02, b_{\text{MS}} = 0.04]$. The metallicity inhibition of SNe Ia at $[Fe/H] \leq -1.1$ is included (49). These parameter can be determined uniquely from the metallicity distribution function and the $[O/Fe]$ - $[Fe/H]$ evolutionary trend at $[Fe/H] \gtrsim -1$ (87; 63).

Figures 12 shows the evolutions of heavy element abundance ratios $[X/Fe]$ against $[Fe/H]$. We note (51; 52):

Oxygen — In our model, $[O/Fe] \sim 0.41$ at $[Fe/H] \sim -1$ and slightly increases

to 0.55 at $[\text{Fe}/\text{H}] \sim -3$. The gradual increase in $[\text{O}/\text{Fe}]$ with decreasing $[\text{Fe}/\text{H}]$ is due to the increasing contributions of more massive, metal-poor SNe II and HNe. The metallicity dependence is as small as 0.2 dex between $Z = Z_\odot$ and $Z = 0$. The mass dependence is larger, but such dependence is weakened because HNe produce more Fe. From $[\text{Fe}/\text{H}] \sim -1$, $[\text{O}/\text{Fe}]$ decreases quickly due to Fe production by SNe Ia (e.g., 63). Further studies of the NLTE and 3D effects on the O-abundance determination are needed (e.g., 6).

Magnesium — Cayrel et al. (15) claimed that $[(\text{Mg}, \text{Si}, \text{Ca}, \text{Ti})/\text{Fe}] \sim 0.2 - 0.3$ being almost constant with a very small dispersion of ~ 0.1 dex. In our model, $[\text{Mg}/\text{Fe}] \sim 0.48$ at $[\text{Fe}/\text{H}] \sim -1$ and slightly increases to 0.62 at $[\text{Fe}/\text{H}] \sim -3$, which is larger than $[\text{Mg}/\text{Fe}] \sim 0.27$ in (15), but in good agreement with the observed relation over the wide range of $[\text{Fe}/\text{H}]$. SNe II with $E_{51} = 1$ typically produce $[\text{Mg}/\text{Fe}] \sim 0.5$ with variation from -0.2 ($Z = Z_\odot$) to 1 ($40M_\odot$).

Silicon and Sulfur — Observed Si abundance is represented by only two lines and affected by the contamination. $[\text{Si}/\text{Fe}]$ is $0.52 - 0.60$ for $-3 \lesssim [\text{Fe}/\text{H}] \lesssim -1$ in our model, which is slightly larger than 0.37 in (15) and other observations. For S, because of the hardness of observation, the plateau value is unknown, and our prediction is $[\text{S}/\text{Fe}] = 0.37 - 0.45$. Some observations suggest a sharp increase with decreasing $[\text{Fe}/\text{H}]$ (41).

Calcium and Titanium — Our model succeeds in reproducing the observation with a plateau $[\text{Ca}/\text{Fe}] \sim 0.31 - 0.39$. However, Ti is by a factor of ~ 0.4 dex underabundant overall, which cannot be improved by changing our parameters. Possible solution to increase Ti is a jet-like explosion with high temperature as discussed in §6 (59).

Sodium, Aluminum, and Copper — The NLTE effect for Na and Al is large for metal-poor stars, and the observational data at $[\text{Fe}/\text{H}] \lesssim -2$ are shifted by -0.2 and $+0.5$, respectively (6). The abundances of odd-Z elements show a strong metallicity dependence. In the one-zone chemical evolution model, however, the decreasing trend of $[(\text{Na}, \text{Al}, \text{Cu})/\text{Fe}]$ toward lower $[\text{Fe}/\text{H}]$ is seen more weakly because of the following mass dependence. Although the timescale when $[\text{Fe}/\text{H}]$ reaches -4 corresponds to the lifetime of $\sim 8M_\odot$, the SFR is peaked at ~ 8 Gyr and stars are forming, and thus more massive stars contribute for lower metallicity. $[\text{Na}/\text{Fe}]$ for $25 - 30M_\odot$, $Z = 0.001$ and $[\text{Al}/\text{Fe}]$ for $40M_\odot$, $Z = 0 - 0.001$ are as large as ~ 0.5 , which contribute at $[\text{Fe}/\text{H}] \lesssim -2.5$.

Chromium, Manganese, Cobalt, and Nickel — As seen in Figure 6, the decreasing trend of $[(\text{Cr}, \text{Mn})/\text{Fe}]$ and the increasing trend of $[\text{Co}/\text{Fe}]$ toward lower $[\text{Fe}/\text{H}]$ are reproduced by invoking the energy dependence of nucleosynthesis (112; 104) in the SN-induced star formation model. In the homogeneous one-zone model, the average yields do not show such trends. From $[\text{Fe}/\text{H}] \sim -1$, SNe Ia contributes to increase $[\text{Mn}/\text{Fe}]$ toward higher metallicity. This is con-

firmed both observationally and theoretically, and Mn can be a key element to discuss SNe Ia contribution, HN fraction, and IMF.

Zinc — Zn is an important element observed in damped Ly α (DLA) systems without the dust depletion effect. At $-2 \lesssim [\text{Fe}/\text{H}] \lesssim -1$, $[\text{Zn}/\text{Fe}]$ is constant to be ~ 0.1 , and mildly decreases to ~ 0 from $[\text{Fe}/\text{H}] \sim -1$ due to SNe Ia, which are consistent with observations. The increasing trend of $[\text{Zn}/\text{Fe}]$ toward lower metallicity (89; 15) cannot be explained by homogeneously mixed model, but needs to introduce inhomogeneous models, i.e., SN-induced star formation.

9 Concluding Remarks

We have calculated the nucleosynthesis yields for various stellar masses, explosion energies, and metallicities (104). From the light curve and spectra fitting of individual supernova, the relations between the mass of the progenitor, explosion energy, and produced ^{56}Ni mass (which decayed to ^{56}Fe) have been obtained. Comparison with the abundance patterns of HMP/EMP/VMP stars has also provided excellent opportunities to test the explosion models and their nucleosynthesis.

Nucleosynthesis yields of these SNe and HNe are in better agreement with the observations than before. In particular, the large Zn and Co abundances and the small Mn and Cr abundances observed in very metal-poor stars (Fig. 6) (104)) can better be explained by introducing HNe. This would imply that HNe have made significant contributions to the early Galactic chemical evolution,

In theoretical models, some element ratios, such as (K, Sc, Ti, V)/Fe, are too small, while some ratios such as Cr/Fe are too large compared with the observed abundance ratios (15). Underproduction of Sc and K may require significantly higher entropy environment for nucleosynthesis, e.g., the “low density” progenitor models for K, Sc, and Ti (112). GRBs would have possible nucleosynthesis site, such as accretion disks around the black hole (90).

We need to investigate the uncertainties in the reaction rates which would be important for synthesis of K and Cr (or ^{52}Fe that decays into ^{52}Cr). Rates of some weak processes would need to be refined in view of critical importance of Y_e near the mass cut. In particular, neutrino processes in the deepest layers of SN ejecta near the mass cut, and accretion disk onto a black hole, would open a new window for SN nucleosynthesis (90; 25; 26; 113).

This work has been supported in part by the Grant-in-Aid for Scientific Research (16540229, 17030005, 17033002, 18104003, 18540231) and the 21st Century COE Program (QUEST) from the JSPS and MEXT of Japan.

Table 2

The yields of individual SN models.

$Z = 0$	13	15	18	20	25	30	40
M	1	1	1	1	1	1	1
E	1	1	1	1	1	1	1
M_{cut}	1.57	1.48	1.65	1.66	1.92	2.07	2.89
p	6.59E+00	7.58E+00	8.43E+00	8.77E+00	1.06E+01	1.17E+01	1.40E+01
d	1.49E-16	1.69E-16	1.28E-16	1.28E-16	2.02E-16	1.34E-16	3.46E-16
^3He	4.12E-05	4.09E-05	3.33E-05	4.76E-05	2.11E-04	2.06E-04	2.56E-05
^4He	4.01E+00	4.40E+00	5.42E+00	5.94E+00	8.03E+00	9.52E+00	1.19E+01
^6Li	3.65E-23	1.11E-22	4.37E-23	3.65E-21	2.69E-21	1.13E-22	7.54E-22
^7Li	2.17E-10	2.94E-10	7.34E-11	2.79E-10	5.68E-09	2.36E-08	3.76E-11
^9Be	1.77E-20	3.22E-22	1.05E-22	4.49E-23	1.24E-17	1.26E-20	5.33E-20
^{10}B	2.92E-21	8.30E-20	3.92E-21	1.57E-19	2.87E-18	5.18E-20	2.37E-17
^{11}B	2.94E-16	3.30E-16	7.14E-16	6.54E-17	9.46E-16	3.27E-15	3.07E-14
^{12}C	7.41E-02	1.72E-01	2.18E-01	2.11E-01	2.94E-01	3.37E-01	4.29E-01
^{13}C	8.39E-08	6.21E-08	2.63E-09	1.14E-08	1.47E-08	1.02E-08	3.21E-09
^{14}N	1.83E-03	1.86E-03	1.89E-04	5.42E-05	5.91E-04	1.64E-06	5.89E-07
^{15}N	6.38E-08	6.86E-08	2.40E-08	1.13E-08	1.17E-07	1.67E-08	6.29E-07
^{16}O	4.50E-01	7.73E-01	1.38E+00	2.11E+00	2.79E+00	4.81E+00	8.38E+00
^{17}O	1.69E-06	1.57E-06	2.79E-07	6.83E-08	1.49E-06	1.88E-08	1.42E-09
^{18}O	5.79E-08	4.89E-06	4.63E-06	2.52E-08	6.75E-07	2.06E-09	2.13E-07
^{19}F	1.17E-10	1.97E-09	7.91E-09	1.62E-09	1.71E-09	8.94E-10	2.38E-10
^{20}Ne	1.53E-02	3.27E-01	4.94E-01	9.12E-01	5.33E-01	8.51E-01	3.07E-01
^{21}Ne	5.42E-07	3.76E-05	9.12E-05	4.30E-05	1.33E-05	5.51E-05	1.08E-05
^{22}Ne	1.98E-07	1.61E-05	2.57E-05	6.92E-05	2.02E-05	8.57E-05	6.75E-06
^{23}Na	1.44E-04	2.45E-03	2.08E-03	2.90E-03	1.03E-03	1.42E-03	1.84E-04
^{24}Mg	8.62E-02	6.82E-02	1.57E-01	1.50E-01	1.20E-01	2.26E-01	4.78E-01
^{25}Mg	1.56E-04	2.98E-04	5.83E-04	1.16E-04	3.97E-05	2.44E-04	4.28E-04
^{26}Mg	7.07E-05	3.98E-04	8.73E-04	2.38E-04	5.01E-05	1.29E-04	1.25E-04
^{26}Al	9.91E-07	1.11E-06	3.33E-06	4.98E-07	7.50E-07	2.92E-06	1.39E-06
^{27}Al	3.78E-03	1.37E-03	3.14E-03	1.37E-03	8.08E-04	2.63E-03	1.47E-02
^{28}Si	8.04E-02	7.32E-02	1.16E-01	9.94E-02	3.51E-01	2.48E-01	1.02E+00
^{29}Si	7.50E-04	2.39E-04	4.42E-04	1.82E-04	2.71E-04	5.88E-04	2.60E-03
^{30}Si	1.42E-03	1.49E-04	3.45E-04	1.10E-04	7.54E-05	2.55E-04	4.06E-03
^{31}P	4.88E-04	5.63E-05	1.32E-04	8.01E-05	8.47E-05	1.17E-04	1.60E-03
^{32}S	2.37E-02	3.20E-02	4.07E-02	5.31E-02	1.85E-01	1.16E-01	3.73E-01
^{33}S	8.98E-05	7.55E-05	1.03E-04	1.98E-04	2.74E-04	1.65E-04	8.10E-04
^{34}S	2.79E-04	2.02E-04	2.85E-04	4.90E-04	4.24E-04	8.42E-05	1.59E-03
^{36}S	1.48E-08	1.43E-09	5.34E-09	2.56E-09	3.41E-10	7.04E-10	3.19E-08
^{35}Cl	5.48E-05	1.46E-05	2.64E-05	6.88E-05	5.42E-05	2.30E-05	2.16E-04
^{37}Cl	3.04E-06	5.83E-06	9.12E-06	3.86E-05	6.11E-05	1.54E-05	9.66E-05
^{36}Ar	3.24E-03	5.28E-03	5.67E-03	9.67E-03	3.10E-02	1.96E-02	4.87E-02
^{38}Ar	5.23E-05	6.23E-05	1.70E-04	3.86E-04	3.59E-04	3.48E-05	1.11E-03
^{40}Ar	8.01E-11	1.78E-11	3.96E-11	1.06E-10	1.77E-11	4.66E-12	1.29E-10
^{39}K	5.02E-06	7.86E-06	1.93E-05	4.40E-05	6.30E-05	1.30E-05	1.18E-04
^{40}K	1.14E-09	9.10E-10	1.96E-09	1.30E-08	8.04E-09	9.94E-10	1.04E-08
^{41}K	3.54E-07	8.05E-07	1.72E-06	9.47E-06	2.08E-05	3.39E-06	2.80E-05
^{40}Ca	2.92E-03	4.41E-03	4.40E-03	6.22E-03	2.48E-02	1.74E-02	3.73E-02
^{42}Ca	9.77E-07	1.23E-06	3.62E-06	1.28E-05	7.46E-06	8.62E-07	2.17E-05
^{43}Ca	6.46E-08	4.93E-08	3.39E-08	7.43E-08	1.58E-08	1.93E-09	9.65E-09
^{44}Ca	1.68E-05	2.21E-05	1.45E-05	1.45E-05	9.79E-06	5.44E-06	8.71E-06
^{46}Ca	1.07E-12	1.76E-12	9.27E-12	1.30E-10	2.78E-11	6.05E-13	5.20E-12
^{48}Ca	1.55E-17	4.21E-14	4.12E-16	4.40E-16	1.26E-11	3.55E-16	1.30E-17
^{45}Sc	2.12E-08	4.03E-08	5.54E-08	2.55E-07	6.16E-07	1.51E-07	5.81E-07
^{46}Ti	6.28E-06	2.71E-06	4.06E-06	5.98E-06	3.18E-06	5.28E-07	1.08E-05
^{47}Ti	8.76E-06	3.86E-06	5.30E-06	4.26E-06	5.90E-08	3.80E-08	9.30E-08
^{48}Ti	6.34E-05	8.39E-05	7.65E-05	8.86E-05	1.55E-04	1.80E-04	2.45E-04
^{49}Ti	2.27E-06	3.32E-06	3.00E-06	3.94E-06	7.04E-06	8.84E-06	1.20E-05
^{50}Ti	1.18E-12	9.55E-13	1.72E-12	1.83E-12	2.24E-12	4.59E-14	9.41E-12
^{50}V	1.35E-11	1.05E-11	4.60E-11	1.36E-10	1.17E-10	2.64E-12	6.53E-10
^{51}V	1.65E-05	1.08E-05	1.24E-05	1.10E-05	9.01E-06	1.06E-05	1.76E-05
^{50}Cr	1.04E-05	1.55E-05	2.64E-05	2.22E-05	4.88E-05	3.82E-05	1.78E-04
^{52}Cr	8.80E-04	1.09E-03	1.13E-03	1.36E-03	2.77E-03	3.12E-03	3.95E-03
^{53}Cr	4.96E-05	6.76E-05	6.43E-05	8.28E-05	1.50E-04	1.82E-04	2.61E-04
^{54}Cr	2.35E-10	4.13E-10	3.25E-09	3.18E-09	9.32E-09	1.72E-10	8.59E-08
^{55}Mn	1.33E-04	1.85E-04	1.74E-04	2.26E-04	4.30E-04	5.16E-04	7.15E-04
^{54}Fe	7.29E-04	1.24E-03	1.40E-03	1.42E-03	3.31E-03	4.09E-03	9.30E-03
^{56}Fe	7.00E-02	7.00E-02	7.00E-02	7.00E-02	7.00E-02	7.00E-02	7.02E-02
^{57}Fe	9.97E-04	1.14E-03	8.78E-04	8.67E-04	4.67E-04	4.83E-04	5.01E-04
^{58}Fe	5.67E-11	1.76E-10	8.07E-10	1.05E-09	2.31E-09	2.26E-10	1.41E-08
^{59}Co	1.76E-04	1.32E-04	1.61E-04	1.50E-04	1.57E-05	2.47E-06	1.87E-06
^{58}Ni	3.85E-04	4.14E-04	3.83E-04	3.78E-04	2.93E-04	3.82E-04	5.74E-04
^{60}Ni	2.12E-03	1.62E-03	1.57E-03	1.34E-03	1.48E-04	3.60E-06	4.38E-06
^{61}Ni	3.61E-05	3.14E-05	2.12E-05	1.85E-05	5.77E-07	6.04E-09	1.32E-09
^{62}Ni	1.94E-05	1.51E-05	1.35E-05	1.19E-05	3.88E-07	1.64E-09	5.36E-10
^{64}Ni	3.83E-15	9.97E-14	1.09E-14	6.10E-14	3.27E-12	3.26E-14	7.71E-15
^{63}Cu	4.89E-06	3.54E-06	3.92E-06	3.44E-06	1.23E-07	2.37E-10	2.06E-11
^{65}Cu	2.14E-07	2.42E-07	1.63E-07	1.42E-07	7.79E-09	1.03E-12	1.30E-13
^{64}Zn	1.25E-04	1.22E-04	9.50E-05	8.29E-05	2.54E-06	3.02E-10	4.36E-11
^{66}Zn	6.84E-07	1.07E-06	5.05E-07	4.24E-07	1.59E-08	3.53E-12	5.14E-13
^{67}Zn	1.62E-08	2.33E-08	1.30E-08	1.05E-08	2.16E-10	6.31E-13	8.47E-14
^{68}Zn	2.94E-08	3.24E-08	4.02E-08	3.43E-08	8.05E-10	1.30E-12	2.62E-13
^{70}Zn	6.94E-16	3.59E-14	6.59E-15	2.51E-14	3.97E-14	1.86E-14	4.45E-16
^{69}Ga	7.81E-09	5.62E-09	6.10E-09	4.93E-09	8.74E-11	5.06E-13	4.26E-15
^{71}Ga	8.53E-15	1.12E-13	1.84E-14	9.21E-14	2.24E-13	2.34E-14	1.36E-15

$Z = 0.001$							
M	13	15	18	20	25	30	40
E	1	1	1	1	1	1	1
M_{cut}	1.65	1.53	1.70	1.85	1.91	2.06	3.17
p	6.44E+00	7.45E+00	8.46E+00	8.43E+00	9.80E+00	1.10E+01	1.29E+01
d	7.19E-15	3.38E-12	3.07E-15	4.35E-16	4.46E-16	5.03E-16	7.03E-14
^3He	1.43E-04	1.53E-04	1.57E-04	1.60E-04	1.26E-04	1.44E-04	1.21E-04
^4He	3.86E+00	5.16E+00	6.54E+00	5.94E+00	6.97E+00	8.38E+00	1.09E+01
^6Li	2.37E-17	1.11E-17	8.84E-18	2.40E-23	2.35E-21	2.75E-23	2.29E-16
^7Li	6.34E-10	3.76E-13	5.83E-13	8.47E-11	9.12E-13	1.12E-12	6.68E-12
^9Be	2.33E-17	9.06E-16	9.32E-17	1.43E-23	2.05E-25	0.00E+00	4.06E-16
^{10}B	1.15E-11	6.01E-12	6.57E-12	2.37E-12	7.60E-12	2.25E-12	2.01E-12
^{11}B	5.11E-11	2.68E-11	2.94E-11	1.03E-11	3.42E-11	1.01E-11	7.01E-12
^{12}C	1.07E-01	8.50E-02	1.29E-01	1.28E-01	2.15E-01	1.21E-01	7.37E-02
^{13}C	1.67E-04	5.38E-05	7.20E-05	1.96E-05	9.81E-05	8.20E-05	2.82E-04
^{14}N	9.07E-03	3.58E-03	4.47E-03	1.29E-02	9.20E-03	6.19E-03	8.69E-03
^{15}N	7.57E-06	8.59E-07	9.21E-07	1.37E-06	7.24E-06	3.79E-07	2.44E-06
^{16}O	5.04E-01	2.94E-01	4.22E-01	2.18E+00	3.82E+00	5.33E+00	8.37E+00
^{17}O	6.96E-05	2.56E-05	2.42E-05	2.18E-05	2.79E-05	4.87E-05	2.86E-05
^{18}O	1.81E-03	3.66E-04	3.06E-04	8.09E-06	7.05E-05	2.69E-05	2.63E-05
^{19}F	3.07E-06	1.98E-07	3.32E-07	2.80E-06	6.12E-07	2.39E-06	4.47E-06
^{20}Ne	6.60E-02	1.90E-01	1.77E-01	6.27E-01	1.22E+00	1.45E+00	2.87E-01
^{21}Ne	1.85E-04	6.75E-05	8.76E-05	1.37E-04	5.09E-04	6.11E-04	1.11E-04
^{22}Ne	1.33E-03	2.74E-04	4.75E-04	1.17E-03	1.47E-03	1.56E-03	8.76E-04
^{23}Na	5.41E-04	1.96E-03	2.09E-03	1.81E-03	8.09E-03	6.86E-03	9.00E-04
^{24}Mg	6.36E-02	6.37E-02	5.93E-02	2.42E-01	1.79E-01	2.86E-01	7.04E-01
^{25}Mg	1.40E-03	8.80E-04	9.46E-04	2.40E-03	1.74E-03	3.55E-03	2.21E-03
^{26}Mg	8.24E-04	1.14E-03	9.24E-04	2.43E-03	1.99E-03	4.26E-03	1.10E-03
^{26}Al	1.01E-05	1.83E-06	3.11E-06	3.57E-06	2.78E-06	7.66E-06	5.00E-06
^{27}Al	3.57E-03	2.35E-03	2.31E-03	6.98E-03	5.05E-03	8.73E-03	3.01E-02
^{28}Si	8.99E-02	4.29E-02	1.53E-01	1.28E-01	1.20E-01	1.65E-01	8.81E-01
^{29}Si	1.42E-03	3.82E-04	6.01E-04	1.11E-03	4.40E-04	1.03E-03	6.04E-03
^{30}Si	1.85E-03	4.25E-04	5.34E-04	7.76E-04	2.75E-04	7.09E-04	1.01E-02
^{31}P	5.31E-04	8.12E-05	1.87E-04	1.97E-04	1.07E-04	2.04E-04	3.48E-03
^{32}S	3.70E-02	1.64E-02	7.88E-02	5.62E-02	5.51E-02	7.80E-02	3.29E-01
^{33}S	1.96E-04	4.76E-05	3.01E-04	9.90E-05	8.12E-05	1.39E-04	8.37E-04
^{34}S	9.22E-04	2.39E-04	6.37E-04	3.10E-04	1.79E-04	3.68E-04	2.12E-03
^{36}S	7.49E-07	1.55E-07	3.20E-07	4.05E-07	6.53E-07	9.04E-07	5.56E-07
^{35}Cl	8.16E-05	8.10E-06	8.16E-05	2.33E-05	2.10E-05	3.35E-05	3.52E-04
^{37}Cl	1.44E-05	2.63E-06	4.13E-05	1.02E-05	1.29E-05	1.92E-05	6.31E-05
^{36}Ar	5.69E-03	2.46E-03	1.22E-02	1.01E-02	9.29E-03	1.35E-02	4.56E-02
^{38}Ar	2.68E-04	2.26E-05	4.12E-04	1.07E-04	8.25E-05	1.63E-04	8.37E-04
^{40}Ar	1.76E-07	4.90E-08	1.03E-07	5.43E-08	9.81E-08	1.18E-07	6.83E-08
^{39}K	2.51E-05	4.15E-06	5.69E-05	1.39E-05	1.52E-05	2.37E-05	1.11E-04
^{40}K	2.66E-08	1.95E-09	3.92E-08	7.57E-09	9.91E-09	9.51E-09	2.38E-08
^{41}K	2.41E-06	3.13E-07	1.09E-05	2.07E-06	2.22E-06	3.98E-06	1.52E-05
^{40}Ca	4.73E-03	1.73E-03	8.06E-03	9.20E-03	7.94E-03	1.17E-02	3.66E-02
^{42}Ca	6.62E-06	4.05E-07	1.35E-05	2.79E-06	2.49E-06	4.64E-06	2.29E-05
^{43}Ca	4.15E-07	3.35E-07	2.45E-07	1.91E-07	2.90E-07	3.55E-07	2.81E-07
^{44}Ca	2.48E-05	2.07E-05	1.87E-05	4.88E-06	7.96E-06	6.44E-06	1.10E-05
^{46}Ca	6.65E-08	1.41E-08	2.55E-08	3.35E-08	3.02E-08	7.09E-08	1.22E-07
^{48}Ca	3.16E-07	9.66E-08	1.22E-07	1.25E-07	1.57E-07	1.86E-07	2.17E-07
^{45}Sc	2.52E-07	5.08E-08	3.55E-07	2.16E-07	3.24E-07	4.22E-07	9.92E-07
^{46}Ti	3.98E-06	1.24E-05	5.11E-06	1.36E-06	1.31E-06	2.15E-06	9.99E-06
^{47}Ti	2.55E-06	1.28E-05	1.50E-06	4.30E-07	3.36E-07	4.50E-07	6.35E-07
^{48}Ti	9.68E-05	5.19E-05	9.98E-05	1.37E-04	1.17E-04	1.67E-04	2.53E-04
^{49}Ti	3.85E-06	1.94E-06	4.13E-06	6.78E-06	5.68E-06	8.43E-06	1.40E-05
^{50}Ti	6.32E-07	1.62E-07	1.86E-07	5.05E-07	8.49E-07	1.14E-06	1.16E-06
^{50}V	1.10E-08	1.12E-09	1.81E-09	8.49E-09	1.31E-08	2.06E-08	9.25E-08
^{51}V	8.95E-05	1.62E-05	7.56E-06	8.23E-06	7.52E-06	9.95E-06	1.94E-05
^{50}Cr	2.10E-05	1.33E-05	2.99E-05	2.37E-05	2.75E-05	3.51E-05	1.35E-04
^{52}Cr	1.20E-03	3.03E-04	1.52E-03	2.22E-03	2.18E-03	2.92E-03	3.94E-03
^{53}Cr	7.43E-05	2.82E-05	9.06E-05	1.37E-04	1.11E-04	1.77E-04	2.56E-04
^{54}Cr	1.87E-06	4.80E-07	5.96E-07	1.41E-06	2.18E-06	2.74E-06	2.84E-06
^{55}Mn	2.27E-04	8.01E-05	2.81E-04	3.80E-04	2.99E-04	5.01E-04	7.86E-04
^{54}Fe	1.53E-03	7.07E-04	2.06E-03	2.37E-03	2.25E-03	3.31E-03	1.04E-02
^{56}Fe	7.26E-02	7.08E-02	7.11E-02	7.09E-02	7.11E-02	7.12E-02	7.15E-02
^{57}Fe	1.41E-03	1.75E-03	1.27E-03	7.21E-04	5.30E-04	5.83E-04	5.75E-04
^{58}Fe	5.68E-05	1.31E-05	1.55E-05	4.99E-05	7.78E-05	9.28E-05	1.02E-04
^{59}Co	8.91E-05	2.32E-04	6.30E-05	6.21E-05	3.42E-05	5.39E-05	4.42E-05
^{58}Ni	5.09E-04	9.11E-04	1.76E-03	3.54E-04	2.51E-04	3.79E-04	7.80E-04
^{60}Ni	1.62E-03	2.57E-03	1.17E-03	2.95E-04	6.57E-05	1.94E-04	1.01E-04
^{61}Ni	5.05E-05	6.92E-05	4.63E-05	1.22E-05	1.57E-05	2.10E-05	2.06E-05
^{62}Ni	1.01E-04	1.87E-04	2.97E-04	2.53E-05	3.71E-05	5.15E-05	7.60E-05
^{64}Ni	1.62E-05	1.83E-06	2.30E-06	2.37E-05	4.32E-05	6.46E-05	7.83E-05
^{63}Cu	8.05E-06	5.47E-06	2.78E-06	9.64E-06	1.44E-05	1.97E-05	1.40E-05
^{65}Cu	4.85E-06	8.85E-07	1.14E-06	8.05E-06	1.49E-05	2.23E-05	2.90E-05
^{64}Zn	7.15E-05	6.50E-05	5.32E-05	1.17E-05	9.03E-06	1.61E-05	1.29E-05
^{66}Zn	9.89E-06	3.96E-06	7.73E-06	1.12E-05	1.93E-05	3.09E-05	4.78E-05
^{67}Zn	1.04E-06	1.41E-07	1.87E-07	2.04E-06	3.86E-06	6.06E-06	4.18E-06
^{68}Zn	6.87E-06	5.82E-07	7.86E-07	9.86E-06	1.86E-05	3.15E-05	4.63E-05
^{70}Zn	2.29E-07	1.05E-08	1.75E-08	2.86E-08	2.35E-08	7.37E-08	1.39E-07
^{69}Ga	7.11E-07	7.43E-08	1.13E-07	1.24E-06	2.33E-06	3.73E-06	4.73E-06
^{71}Ga	6.34E-07	5.13E-08	7.70E-08	1.09E-06	2.01E-06	3.84E-06	5.45E-06

$Z = 0.004$							
M	13	15	18	20	25	30	40
E	1	1	1	1	1	1	1
M_{cut}	1.61	1.50	1.61	1.76	1.68	2.56	2.81
p	6.37E+00	7.11E+00	7.47E+00	8.95E+00	1.02E+01	1.01E+01	1.03E+01
d	1.07E-14	1.99E-14	4.57E-14	8.80E-14	3.23E-16	6.93E-14	2.64E-16
^3He	1.70E-04	1.59E-04	2.24E-04	1.75E-04	1.85E-04	1.84E-04	1.80E-04
^4He	4.04E+00	4.95E+00	6.06E+00	7.03E+00	8.48E+00	7.92E+00	8.12E+00
^6Li	3.44E-17	6.50E-17	1.50E-16	2.89E-16	5.19E-23	2.23E-16	2.14E-20
^7Li	3.15E-15	7.20E-14	5.04E-13	1.56E-12	1.02E-13	8.01E-13	4.71E-12
^9Be	1.07E-16	1.08E-16	1.58E-16	5.51E-16	4.88E-24	3.78E-16	6.00E-22
^{10}B	2.55E-11	2.55E-11	1.55E-10	2.91E-11	3.09E-11	3.04E-11	6.57E-12
^{11}B	1.15E-10	1.15E-10	6.97E-10	4.60E-08	1.39E-10	1.37E-10	2.80E-11
^{12}C	8.78E-02	8.81E-02	1.05E-01	9.74E-02	1.32E-01	1.82E-01	4.58E-01
^{13}C	1.88E-04	2.09E-04	6.03E-02	2.92E-04	3.82E-04	3.39E-04	3.68E-04
^{14}N	9.08E-03	1.29E-02	7.27E-02	1.84E-02	3.15E-02	2.00E-02	2.60E-02
^{15}N	6.84E-06	8.70E-06	5.35E-02	2.78E-05	9.53E-05	4.98E-06	5.01E-06
^{16}O	3.85E-01	2.92E-01	5.21E-01	9.94E-01	2.20E+00	4.79E+00	7.96E+00
^{17}O	8.75E-05	8.66E-05	1.11E-03	1.04E-04	1.12E-04	1.20E-04	1.59E-04
^{18}O	1.95E-03	9.68E-04	5.20E-02	1.28E-03	8.48E-04	4.35E-05	8.37E-04
^{19}F	1.98E-06	2.13E-06	1.21E-05	5.36E-06	8.50E-05	1.16E-05	1.04E-06
^{20}Ne	1.32E-01	1.24E-01	2.00E-01	2.77E-01	8.20E-01	9.37E-01	1.88E+00
^{21}Ne	1.85E-04	1.43E-04	1.00E-03	2.58E-04	3.83E-04	7.21E-04	1.17E-03
^{22}Ne	1.05E-03	7.54E-04	4.17E-03	2.16E-03	4.57E-03	6.18E-03	2.87E-03
^{23}Na	1.50E-03	8.19E-04	6.63E-03	4.07E-03	6.25E-03	1.41E-02	2.61E-02
^{24}Mg	4.38E-02	7.46E-02	6.93E-02	9.65E-02	2.33E-01	2.18E-01	3.79E-01
^{25}Mg	1.38E-03	1.95E-03	8.19E-03	2.20E-03	6.04E-03	7.09E-03	1.20E-02
^{26}Mg	1.24E-03	1.93E-03	6.44E-03	1.88E-03	6.71E-03	7.07E-03	1.33E-02
^{26}Al	2.68E-06	4.79E-06	2.26E-05	8.65E-06	3.69E-06	1.18E-05	2.23E-05
^{27}Al	2.21E-03	3.31E-03	6.29E-03	5.13E-03	1.12E-02	1.69E-02	3.04E-02
^{28}Si	6.11E-02	1.03E-01	9.41E-02	1.24E-01	1.19E-01	3.95E-01	5.23E-01
^{29}Si	5.41E-04	1.12E-03	2.70E-03	1.27E-03	1.93E-03	3.37E-03	4.55E-03
^{30}Si	6.56E-04	1.29E-03	3.89E-03	1.61E-03	1.58E-03	4.82E-03	6.50E-03
^{31}P	1.50E-04	2.74E-04	7.36E-04	3.87E-04	3.86E-04	1.02E-03	1.48E-03
^{32}S	2.68E-02	3.44E-02	4.07E-02	5.15E-02	3.48E-02	1.90E-01	2.26E-01
^{33}S	9.09E-05	1.83E-04	2.62E-04	1.89E-04	1.66E-04	4.34E-04	4.55E-04
^{34}S	4.27E-04	9.56E-04	2.38E-03	9.12E-04	7.22E-04	2.03E-03	2.35E-03
^{36}S	7.10E-07	9.91E-07	7.79E-06	1.36E-06	2.68E-06	6.10E-06	1.19E-05
^{35}Cl	2.66E-05	5.21E-05	1.09E-04	5.46E-05	5.30E-05	1.23E-04	1.56E-04
^{37}Cl	1.01E-05	1.65E-05	4.60E-05	2.05E-05	3.03E-05	7.79E-05	1.13E-04
^{36}Ar	4.50E-03	4.31E-03	6.96E-03	7.99E-03	4.73E-03	3.09E-02	3.48E-02
^{38}Ar	1.66E-04	4.94E-04	7.43E-04	3.06E-04	2.67E-04	9.77E-04	1.14E-03
^{40}Ar	2.30E-07	3.74E-07	2.55E-06	3.30E-07	3.57E-07	9.25E-07	1.15E-06
^{39}K	1.78E-05	3.20E-05	7.20E-05	3.12E-05	2.64E-05	1.02E-04	9.93E-05
^{40}K	7.78E-09	9.13E-09	6.68E-08	1.85E-08	3.34E-08	7.91E-08	7.41E-08
^{41}K	1.87E-06	2.46E-06	7.11E-06	3.13E-06	3.43E-06	1.30E-05	1.35E-05
^{40}Ca	3.91E-03	3.08E-03	6.12E-03	6.50E-03	3.77E-03	2.59E-02	2.83E-02
^{42}Ca	4.16E-06	9.59E-06	1.81E-05	7.31E-06	6.00E-06	2.65E-05	2.98E-05
^{43}Ca	3.41E-07	3.60E-07	1.93E-06	5.23E-07	7.95E-07	9.89E-07	1.43E-06
^{44}Ca	2.07E-05	2.30E-05	3.40E-05	2.09E-05	2.65E-05	1.51E-05	1.88E-05
^{46}Ca	7.37E-08	1.18E-07	6.81E-07	1.10E-07	1.28E-07	1.97E-07	3.24E-07
^{48}Ca	3.22E-07	4.02E-07	2.37E-06	5.02E-07	6.19E-07	6.48E-07	7.80E-07
^{45}Sc	2.16E-07	2.48E-07	1.35E-06	3.61E-07	5.30E-07	1.09E-06	1.64E-06
^{46}Ti	5.16E-06	6.09E-06	8.19E-06	3.54E-06	5.14E-06	1.22E-05	1.40E-05
^{47}Ti	5.40E-06	3.40E-06	4.65E-06	1.33E-06	6.46E-06	1.46E-06	2.04E-06
^{48}Ti	8.17E-05	7.41E-05	1.37E-04	1.14E-04	8.94E-05	2.33E-04	2.68E-04
^{49}Ti	3.49E-06	2.81E-06	7.25E-06	5.19E-06	4.09E-06	1.36E-05	1.72E-05
^{50}Ti	5.85E-07	5.61E-07	3.72E-06	1.08E-06	2.25E-06	4.10E-06	7.70E-06
^{50}V	4.61E-09	4.94E-09	4.06E-08	1.01E-08	1.98E-08	5.38E-08	9.68E-08
^{51}V	1.31E-05	9.56E-06	1.23E-05	8.01E-06	1.41E-05	1.77E-05	2.20E-05
^{50}Cr	1.75E-05	2.71E-05	3.34E-05	3.06E-05	2.47E-05	8.56E-05	1.21E-04
^{52}Cr	1.11E-03	9.63E-04	1.81E-03	1.66E-03	1.24E-03	3.73E-03	4.07E-03
^{53}Cr	6.78E-05	5.90E-05	1.23E-04	1.04E-04	7.21E-05	2.43E-04	2.76E-04
^{54}Cr	1.75E-06	1.84E-06	1.07E-05	3.11E-06	5.79E-06	8.65E-06	1.39E-05
^{55}Mn	2.00E-04	1.71E-04	4.68E-04	3.29E-04	2.34E-04	7.61E-04	8.38E-04
^{54}Fe	1.24E-03	1.23E-03	2.63E-03	2.37E-03	1.41E-03	7.09E-03	9.39E-03
^{56}Fe	7.26E-02	7.30E-02	8.72E-02	7.40E-02	7.47E-02	7.46E-02	7.47E-02
^{57}Fe	1.05E-03	1.13E-03	4.00E-03	1.22E-03	1.05E-03	7.15E-04	7.31E-04
^{58}Fe	4.77E-05	4.89E-05	2.66E-04	9.17E-05	1.85E-04	2.89E-04	4.34E-04
^{59}Co	1.96E-04	1.31E-04	2.69E-04	6.21E-05	2.17E-04	1.28E-04	1.91E-04
^{58}Ni	5.14E-04	4.64E-04	2.25E-02	4.93E-04	5.44E-04	7.14E-04	8.27E-04
^{60}Ni	1.80E-03	1.67E-03	1.37E-03	1.29E-03	1.80E-03	2.63E-04	3.80E-04
^{61}Ni	4.25E-05	4.99E-05	2.66E-04	5.67E-05	6.09E-05	5.55E-05	9.80E-05
^{62}Ni	3.55E-05	2.40E-05	3.08E-03	9.09E-05	1.09E-04	1.75E-04	3.01E-04
^{64}Ni	1.09E-05	3.62E-06	6.68E-05	2.79E-05	9.88E-05	1.95E-04	4.25E-04
^{63}Cu	1.05E-05	5.37E-06	3.62E-05	1.35E-05	4.27E-05	5.23E-05	1.04E-04
^{65}Cu	3.81E-06	1.51E-06	2.12E-05	1.02E-05	3.17E-05	6.94E-05	1.45E-04
^{64}Zn	1.14E-04	1.16E-04	2.31E-05	6.04E-05	1.29E-04	2.98E-05	5.80E-05
^{66}Zn	6.72E-06	4.66E-06	8.57E-05	1.71E-05	4.58E-05	1.06E-04	2.18E-04
^{67}Zn	7.89E-07	3.21E-07	5.78E-06	2.25E-06	8.56E-06	1.82E-05	4.11E-05
^{68}Zn	3.52E-06	1.52E-06	2.86E-05	1.17E-05	4.38E-05	1.20E-04	2.64E-04
^{70}Zn	1.12E-07	8.93E-08	1.06E-06	9.23E-08	1.66E-07	4.58E-07	5.82E-07
^{69}Ga	5.06E-07	1.74E-07	2.88E-06	1.55E-06	5.59E-06	1.60E-05	3.37E-05
^{71}Ga	3.05E-07	2.05E-07	2.89E-06	1.17E-06	4.72E-06	1.33E-05	2.92E-05

$Z = 0.02$							
M	13	15	18	20	25	30	40
E	1	1	1	1	1	1	1
M_{cut}	1.60	1.50	1.58	1.55	1.69	2.10	2.21
p	6.15E+00	6.79E+00	7.53E+00	7.93E+00	8.41E+00	8.75E+00	3.55E+00
d	8.34E-15	1.02E-14	4.16E-16	1.20E-15	9.87E-16	1.08E-15	7.71E-17
^3He	1.96E-04	2.18E-04	2.30E-04	2.38E-04	2.21E-04	2.12E-04	5.05E-05
^4He	4.30E+00	5.25E+00	6.11E+00	6.76E+00	7.24E+00	8.36E+00	4.71E+00
^6Li	1.32E-17	3.17E-17	2.78E-19	1.09E-22	9.53E-23	5.90E-23	3.47E-22
^7Li	5.63E-11	7.09E-13	2.80E-13	4.32E-12	6.93E-13	4.33E-13	5.72E-13
^9Be	4.61E-19	1.55E-18	7.56E-18	4.72E-23	2.23E-20	4.92E-23	7.03E-23
^{10}B	1.12E-10	1.36E-10	1.42E-10	1.47E-10	1.51E-10	1.54E-10	6.96E-14
^{11}B	4.28E-10	6.02E-10	6.41E-10	6.54E-10	6.77E-10	6.92E-10	3.22E-14
^{12}C	1.07E-01	6.51E-02	1.36E-01	2.45E-01	1.52E-01	2.50E-01	5.96E-01
^{13}C	1.00E-03	1.15E-03	1.38E-03	1.45E-03	6.66E-02	1.92E-03	4.31E-04
^{14}N	4.80E-02	6.15E-02	6.61E-02	7.19E-02	8.43E-02	1.02E-01	5.81E-02
^{15}N	4.09E-05	5.97E-05	1.53E-05	2.24E-04	4.63E-02	6.55E-06	5.72E-06
^{16}O	2.18E-01	1.62E-01	7.70E-01	1.05E+00	2.35E+00	3.22E+00	7.33E+00
^{17}O	8.68E-04	8.12E-04	8.76E-04	9.51E-04	1.34E-03	1.69E-03	9.72E-04
^{18}O	3.50E-03	2.54E-03	1.17E-02	5.22E-03	8.43E-02	6.18E-03	1.23E-02
^{19}F	1.42E-05	1.64E-05	4.47E-06	6.05E-05	1.19E-04	7.81E-06	5.26E-06
^{20}Ne	3.47E-02	3.39E-02	1.49E-01	3.94E-01	8.53E-01	9.37E-01	2.21E+00
^{21}Ne	2.25E-04	1.30E-04	2.02E-04	1.81E-03	1.59E-03	2.97E-03	4.97E-03
^{22}Ne	4.52E-03	1.72E-03	6.63E-03	9.04E-03	1.68E-02	1.86E-02	1.09E-02
^{23}Na	9.25E-04	1.06E-03	2.93E-03	1.68E-02	1.86E-02	3.47E-02	7.76E-02
^{24}Mg	2.52E-02	3.79E-02	1.03E-01	7.16E-02	2.18E-01	1.88E-01	3.10E-01
^{25}Mg	2.56E-03	1.46E-03	7.08E-03	1.44E-02	3.13E-02	3.12E-02	7.28E-02
^{26}Mg	2.16E-03	1.72E-03	5.86E-03	8.86E-03	2.72E-02	2.79E-02	7.33E-02
^{26}Al	2.13E-05	7.63E-06	3.69E-05	1.50E-05	8.67E-05	3.90E-05	6.64E-05
^{27}Al	1.50E-03	2.44E-03	1.00E-02	9.90E-03	2.70E-02	3.41E-02	8.30E-02
^{28}Si	7.48E-02	8.38E-02	1.01E-01	6.32E-02	1.28E-01	2.40E-01	2.41E-01
^{29}Si	1.49E-03	2.20E-03	6.96E-03	2.04E-03	7.06E-03	7.38E-03	9.99E-03
^{30}Si	1.55E-03	2.75E-03	6.82E-03	2.44E-03	6.19E-03	1.06E-02	9.76E-03
^{31}P	3.75E-04	7.06E-04	1.74E-03	6.58E-04	1.50E-03	2.56E-03	3.52E-03
^{32}S	3.73E-02	3.47E-02	3.69E-02	2.81E-02	4.99E-02	1.08E-01	1.09E-01
^{33}S	2.00E-04	2.43E-04	3.51E-04	2.26E-04	3.25E-04	4.81E-04	4.81E-04
^{34}S	1.64E-03	1.53E-03	2.19E-03	1.70E-03	2.26E-03	3.76E-03	3.42E-03
^{36}S	5.37E-06	2.54E-06	1.20E-05	9.19E-06	2.42E-05	5.09E-05	9.40E-05
^{35}Cl	1.15E-04	1.37E-04	1.75E-04	1.25E-04	1.62E-04	2.33E-04	2.76E-04
^{37}Cl	3.03E-05	2.49E-05	5.65E-05	8.42E-05	1.70E-04	2.63E-04	5.64E-04
^{36}Ar	6.29E-03	4.90E-03	5.48E-03	4.66E-03	7.92E-03	1.81E-02	1.81E-02
^{38}Ar	6.86E-04	6.51E-04	7.83E-04	6.74E-04	8.98E-04	1.64E-03	1.65E-03
^{40}Ar	8.96E-07	1.05E-06	1.30E-06	1.41E-06	2.68E-06	7.41E-06	5.67E-06
^{39}K	5.02E-05	7.00E-05	7.67E-05	7.39E-05	8.83E-05	1.29E-04	1.14E-04
^{40}K	1.28E-07	6.43E-08	1.38E-07	9.30E-08	2.00E-07	2.94E-07	4.05E-07
^{41}K	4.68E-06	5.85E-06	7.74E-06	9.03E-06	1.39E-05	1.97E-05	4.52E-05
^{40}Ca	4.92E-03	4.01E-03	4.54E-03	3.74E-03	6.55E-03	1.57E-02	1.56E-02
^{42}Ca	1.39E-05	1.75E-05	2.07E-05	1.74E-05	2.47E-05	4.15E-05	4.48E-05
^{43}Ca	1.36E-06	1.50E-06	2.12E-06	2.52E-06	3.42E-06	2.97E-06	4.93E-06
^{44}Ca	3.51E-05	3.55E-05	5.45E-05	5.79E-05	5.11E-05	4.04E-05	4.67E-05
^{46}Ca	2.12E-07	3.33E-07	7.83E-07	6.15E-07	1.18E-06	1.18E-06	2.86E-06
^{48}Ca	1.58E-06	1.86E-06	2.73E-06	2.35E-06	2.73E-06	1.42E-05	2.43E-06
^{45}Sc	7.29E-07	9.30E-07	1.26E-06	1.30E-06	2.80E-06	2.57E-06	6.15E-06
^{46}Ti	6.01E-06	8.64E-06	9.50E-06	8.53E-06	1.13E-05	1.86E-05	2.11E-05
^{47}Ti	4.41E-06	3.44E-06	5.34E-06	6.55E-06	5.59E-06	8.81E-06	6.75E-06
^{48}Ti	8.13E-05	1.07E-04	1.32E-04	1.15E-04	1.53E-04	2.53E-04	2.44E-04
^{49}Ti	4.74E-06	5.07E-06	6.11E-06	6.37E-06	1.10E-05	1.92E-05	2.42E-05
^{50}Ti	2.33E-06	2.41E-06	3.91E-06	5.82E-06	1.23E-05	9.91E-06	3.81E-05
^{50}V	2.03E-08	2.66E-08	6.60E-08	3.89E-08	9.60E-08	2.49E-07	1.87E-07
^{51}V	1.18E-05	9.95E-06	1.14E-05	1.33E-05	1.44E-05	2.50E-05	2.24E-05
^{50}Cr	2.23E-05	3.95E-05	3.68E-05	3.10E-05	5.22E-05	7.71E-05	9.21E-05
^{52}Cr	6.48E-04	1.27E-03	1.28E-03	1.07E-03	2.04E-03	3.76E-03	3.78E-03
^{53}Cr	6.24E-05	9.27E-05	9.62E-05	8.28E-05	1.41E-04	2.74E-04	2.49E-04
^{54}Cr	6.55E-06	6.80E-06	1.52E-05	1.66E-05	2.77E-05	5.12E-05	5.66E-05
^{55}Mn	2.81E-04	3.80E-04	4.05E-04	3.60E-04	5.50E-04	1.04E-03	8.28E-04
^{54}Fe	1.92E-03	2.46E-03	2.49E-03	2.22E-03	3.84E-03	6.87E-03	6.42E-03
^{56}Fe	8.32E-02	8.51E-02	8.72E-02	8.87E-02	9.01E-02	9.18E-02	8.08E-02
^{57}Fe	2.22E-03	1.99E-03	2.67E-03	2.34E-03	1.87E-03	2.82E-03	9.75E-04
^{58}Fe	1.21E-04	1.10E-04	5.86E-04	4.96E-04	8.37E-04	2.39E-03	1.48E-03
^{59}Co	1.41E-04	9.00E-05	1.82E-04	2.92E-04	3.89E-04	5.39E-04	6.94E-04
^{58}Ni	2.23E-03	1.14E-03	2.70E-03	1.84E-03	1.56E-03	1.55E-03	8.83E-04
^{60}Ni	2.13E-03	1.87E-03	2.12E-03	2.49E-03	1.81E-03	6.12E-04	1.20E-03
^{61}Ni	8.21E-05	1.24E-04	1.04E-04	1.49E-04	2.16E-04	1.10E-04	3.91E-04
^{62}Ni	2.27E-04	1.64E-04	4.64E-04	3.86E-04	6.61E-04	2.22E-04	1.17E-03
^{64}Ni	3.35E-05	1.72E-05	2.99E-05	1.87E-04	6.16E-04	7.11E-05	2.22E-03
^{63}Cu	1.83E-05	1.30E-05	1.90E-05	1.28E-04	2.94E-04	8.56E-05	6.85E-04
^{65}Cu	1.03E-05	7.18E-06	7.62E-06	4.40E-05	1.46E-04	1.30E-05	6.49E-04
^{64}Zn	9.67E-05	6.77E-05	5.74E-05	1.20E-04	5.37E-05	1.87E-05	1.68E-04
^{66}Zn	1.74E-05	1.78E-05	2.17E-05	6.26E-05	2.39E-04	1.54E-05	1.07E-03
^{67}Zn	2.88E-06	1.78E-06	2.03E-06	1.29E-05	5.26E-05	2.72E-06	2.48E-04
^{68}Zn	1.32E-05	7.49E-06	1.17E-05	6.03E-05	3.14E-04	1.27E-05	1.55E-03
^{70}Zn	1.83E-06	5.59E-07	5.13E-07	1.62E-06	8.43E-06	3.69E-07	2.65E-05
^{69}Ga	1.67E-06	8.45E-07	9.10E-07	6.66E-06	2.74E-05	1.38E-06	1.75E-04
^{71}Ga	1.48E-06	7.96E-07	1.06E-06	5.14E-06	2.79E-05	1.10E-06	1.32E-04

Z = 0					Z = 0.001				
M	20	25	30	40	M	20	25	30	40
E	10	10	10	10	E	10	10	10	10
M _{cut}	1.87	2.74	3.13	5.43	M _{cut}	2.20	2.09	2.54	5.41
p	8.77E+00	1.06E+01	1.17E+01	1.40E+01	p	8.43E+00	9.80E+00	1.10E+01	1.29E+01
d	8.66E-17	2.06E-16	1.09E-14	1.66E-14	d	4.10E-16	4.46E-16	1.53E-13	2.66E-15
³ He	4.76E-05	2.11E-04	2.06E-04	2.56E-05	³ He	1.60E-04	1.26E-04	1.44E-04	2.11E-04
⁴ He	5.96E+00	8.03E+00	9.54E+00	1.18E+01	⁴ He	5.96E+00	7.00E+00	8.42E+00	1.08E+01
⁶ Li	1.53E-22	3.22E-20	3.50E-17	5.39E-17	⁶ Li	9.37E-22	4.74E-21	5.08E-16	7.65E-18
⁷ Li	2.79E-10	5.68E-09	2.36E-08	3.42E-11	⁷ Li	8.42E-11	9.12E-13	1.12E-12	1.91E-12
⁹ Be	4.83E-20	3.69E-17	3.09E-18	9.03E-18	⁹ Be	1.72E-21	2.54E-25	2.59E-16	1.35E-18
¹⁰ B	1.95E-19	7.45E-14	1.05E-14	9.41E-15	¹⁰ B	2.37E-12	7.60E-12	2.25E-12	2.02E-12
¹¹ B	1.09E-15	1.28E-12	9.53E-14	9.41E-13	¹¹ B	1.05E-11	3.42E-11	1.01E-11	8.36E-12
¹² C	1.90E-01	2.67E-01	3.16E-01	3.72E-01	¹² C	1.24E-01	1.94E-01	1.05E-01	5.08E-02
¹³ C	1.18E-08	6.94E-08	6.32E-08	8.18E-08	¹³ C	1.96E-05	9.81E-05	8.20E-05	2.82E-04
¹⁴ N	5.42E-05	5.96E-04	4.18E-05	3.39E-06	¹⁴ N	1.29E-02	9.20E-03	6.19E-03	8.53E-03
¹⁵ N	2.95E-08	1.75E-07	2.20E-07	6.54E-07	¹⁵ N	1.37E-06	7.24E-06	9.07E-07	3.17E-06
¹⁶ O	2.03E+00	2.38E+00	3.92E+00	6.32E+00	¹⁶ O	2.00E+00	3.70E+00	4.94E+00	6.42E+00
¹⁷ O	7.13E-08	1.49E-06	3.81E-08	1.23E-08	¹⁷ O	2.18E-05	2.79E-05	4.87E-05	2.83E-05
¹⁸ O	2.33E-08	3.87E-07	5.03E-07	2.93E-07	¹⁸ O	8.10E-06	7.05E-05	1.99E-05	1.76E-04
¹⁹ F	2.12E-09	1.67E-09	7.88E-09	1.17E-07	¹⁹ F	2.80E-06	6.07E-07	2.04E-06	1.65E-06
²⁰ Ne	7.49E-01	2.85E-01	5.20E-01	2.64E-01	²⁰ Ne	4.56E-01	1.05E+00	1.04E+00	1.83E-01
²¹ Ne	3.58E-05	1.22E-05	3.51E-05	1.41E-05	²¹ Ne	9.70E-05	4.23E-04	4.43E-04	2.16E-05
²² Ne	5.51E-05	8.62E-06	3.52E-05	1.66E-05	²² Ne	1.17E-03	1.44E-03	1.26E-03	1.25E-04
²³ Na	2.31E-03	4.42E-04	7.36E-04	3.28E-04	²³ Na	1.29E-03	6.76E-03	4.68E-03	6.04E-04
²⁴ Mg	1.65E-01	1.53E-01	2.17E-01	3.37E-01	²⁴ Mg	2.30E-01	1.93E-01	3.11E-01	5.20E-01
²⁵ Mg	1.07E-04	4.57E-05	1.45E-04	5.95E-04	²⁵ Mg	1.74E-03	1.52E-03	2.79E-03	1.64E-03
²⁶ Mg	2.09E-04	3.89E-05	8.00E-05	6.90E-05	²⁶ Mg	1.75E-03	1.75E-03	3.20E-03	8.98E-04
²⁷ Al	1.02E-06	1.28E-06	2.92E-06	3.80E-05	²⁷ Al	4.70E-06	3.67E-06	9.51E-06	2.02E-05
²⁸ Al	1.50E-03	8.93E-04	1.55E-03	7.52E-03	²⁸ Al	6.32E-03	5.17E-03	8.70E-03	1.96E-02
²⁸ Si	1.03E-01	2.31E-01	2.47E-01	7.20E-01	²⁸ Si	1.14E-01	1.12E-01	2.35E-01	7.14E-01
²⁹ Si	2.95E-04	5.38E-04	8.85E-04	3.72E-03	²⁹ Si	1.28E-03	7.80E-04	1.69E-03	6.22E-03
³⁰ Si	1.13E-04	6.35E-05	1.47E-04	2.82E-03	³⁰ Si	1.07E-03	4.86E-04	1.24E-03	8.00E-03
³¹ P	7.67E-05	5.91E-05	1.16E-04	1.01E-03	³¹ P	2.71E-04	1.84E-04	3.95E-04	2.67E-03
³² S	4.27E-02	9.16E-02	8.49E-02	2.59E-01	³² S	3.63E-02	4.25E-02	9.25E-02	8.30E-01
³³ S	1.44E-04	2.31E-04	3.02E-04	8.45E-04	³³ S	1.80E-04	2.13E-04	4.11E-04	1.20E-03
³⁴ S	1.84E-04	1.26E-04	2.70E-04	2.08E-03	³⁴ S	5.11E-04	4.16E-04	1.02E-03	3.74E-03
³⁶ S	8.33E-10	5.78E-11	1.41E-09	5.04E-08	³⁶ S	3.31E-07	5.67E-07	9.40E-07	9.90E-07
³⁵ Cl	3.95E-05	3.23E-05	4.48E-05	1.80E-04	³⁵ Cl	3.80E-05	5.36E-05	1.01E-04	3.55E-04
³⁷ Cl	1.88E-05	2.89E-05	2.39E-05	7.95E-05	³⁷ Cl	1.38E-05	1.92E-05	3.75E-05	8.89E-05
³⁶ Ar	6.80E-03	1.36E-02	1.15E-02	3.55E-02	³⁶ Ar	5.55E-03	6.86E-03	1.40E-02	3.67E-02
³⁸ Ar	1.27E-04	1.70E-04	9.07E-05	7.83E-04	³⁸ Ar	1.43E-04	1.18E-04	3.61E-04	1.24E-03
⁴⁰ Ar	3.79E-11	1.16E-11	1.87E-11	2.68E-10	⁴⁰ Ar	4.52E-08	8.65E-08	2.54E-07	3.89E-07
³⁹ K	2.31E-05	3.76E-05	2.05E-05	1.31E-04	³⁹ K	2.05E-05	1.76E-05	5.43E-05	1.61E-04
⁴⁰ K	4.40E-09	1.40E-09	2.52E-09	1.18E-08	⁴⁰ K	6.87E-09	1.10E-08	1.23E-08	3.11E-08
⁴¹ K	3.72E-06	6.48E-06	3.66E-06	2.13E-05	⁴¹ K	2.64E-06	2.25E-06	7.08E-06	2.06E-05
⁴⁰ Ca	4.77E-03	1.02E-02	8.22E-03	2.86E-02	⁴⁰ Ca	4.49E-03	5.46E-03	1.10E-02	2.93E-02
⁴² Ca	3.41E-06	5.15E-06	1.62E-06	1.97E-05	⁴² Ca	3.70E-06	2.18E-06	8.11E-06	3.10E-05
⁴³ Ca	2.60E-07	7.25E-08	1.71E-07	1.39E-07	⁴³ Ca	3.78E-07	4.93E-07	6.45E-07	4.08E-07
⁴⁴ Ca	1.26E-04	7.04E-05	1.82E-04	1.75E-04	⁴⁴ Ca	1.30E-04	1.33E-04	2.44E-04	1.57E-04
⁴⁶ Ca	1.15E-11	1.47E-11	9.25E-12	3.69E-11	⁴⁶ Ca	2.46E-08	2.66E-08	1.10E-07	1.90E-07
⁴⁸ Ca	3.74E-15	1.17E-11	8.16E-13	1.27E-11	⁴⁸ Ca	1.19E-07	1.51E-07	1.81E-07	2.14E-07
⁴⁵ Sc	1.85E-07	2.20E-07	6.95E-08	6.28E-07	⁴⁵ Sc	2.13E-07	3.18E-07	5.55E-07	1.04E-06
⁴⁶ Ti	6.54E-06	5.22E-06	6.23E-06	1.11E-05	⁴⁶ Ti	3.79E-06	1.34E-05	1.30E-05	1.52E-05
⁴⁷ Ti	9.65E-06	9.45E-06	2.08E-05	2.59E-05	⁴⁷ Ti	4.83E-06	2.80E-05	3.27E-05	1.93E-05
⁴⁸ Ti	1.57E-04	1.35E-04	2.81E-04	3.43E-04	⁴⁸ Ti	1.65E-04	1.80E-04	3.25E-04	3.33E-04
⁴⁹ Ti	2.75E-06	3.62E-06	5.70E-06	6.92E-06	⁴⁹ Ti	2.70E-06	2.74E-06	5.41E-06	8.76E-06
⁵⁰ Ti	7.64E-13	6.12E-12	2.49E-12	3.37E-11	⁵⁰ Ti	4.09E-07	7.50E-07	9.05E-07	7.63E-07
⁵⁰ V	2.62E-11	2.79E-11	9.03E-12	1.20E-10	⁵⁰ V	7.17E-09	1.23E-08	1.72E-08	5.05E-08
⁵¹ V	2.42E-05	1.86E-05	3.71E-05	3.48E-05	⁵¹ V	1.19E-05	5.45E-05	4.73E-05	2.75E-05
⁵⁰ Cr	1.68E-05	2.56E-05	1.90E-05	4.12E-05	⁵⁰ Cr	1.24E-05	2.01E-05	2.68E-05	5.49E-05
⁵² Cr	6.58E-04	1.21E-03	1.51E-03	2.70E-03	⁵² Cr	7.39E-04	8.99E-04	1.53E-03	2.97E-03
⁵³ Cr	3.33E-05	7.24E-05	9.03E-05	1.31E-04	⁵³ Cr	3.97E-05	3.81E-05	7.11E-05	1.63E-04
⁵⁴ Cr	2.61E-09	5.72E-09	9.64E-11	3.52E-09	⁵⁴ Cr	1.15E-06	1.95E-06	2.28E-06	1.97E-06
⁵⁵ Mn	8.22E-05	2.02E-04	2.47E-04	3.68E-04	⁵⁵ Mn	1.09E-04	1.12E-04	1.96E-04	4.66E-04
⁵⁴ Fe	7.18E-04	1.79E-03	1.74E-03	3.30E-03	⁵⁴ Fe	8.40E-04	1.18E-03	1.94E-03	4.06E-03
⁵⁶ Fe	8.24E-02	9.60E-02	1.59E-01	2.56E-01	⁵⁶ Fe	8.06E-02	1.50E-01	2.00E-01	2.59E-01
⁵⁷ Fe	1.78E-03	1.63E-03	3.10E-03	4.24E-03	⁵⁷ Fe	2.05E-03	2.79E-03	3.83E-03	4.21E-03
⁵⁸ Fe	1.28E-09	2.60E-09	9.19E-11	3.31E-09	⁵⁸ Fe	3.93E-05	6.84E-05	7.77E-05	6.60E-05
⁵⁹ Co	3.69E-04	2.38E-04	5.19E-04	5.19E-04	⁵⁹ Co	1.55E-04	6.60E-04	7.86E-04	4.49E-04
⁵⁸ Ni	8.75E-04	6.72E-04	1.27E-03	1.43E-03	⁵⁸ Ni	5.66E-04	1.10E-03	1.69E-03	1.39E-03
⁶⁰ Ni	2.99E-03	2.80E-03	5.49E-03	8.37E-03	⁶⁰ Ni	2.75E-03	6.17E-03	7.02E-03	7.93E-03
⁶¹ Ni	6.29E-05	4.34E-05	8.63E-05	9.87E-05	⁶¹ Ni	8.43E-05	1.14E-04	1.31E-04	1.31E-04
⁶² Ni	4.19E-05	2.86E-05	5.74E-05	6.74E-05	⁶² Ni	5.49E-05	1.03E-04	1.16E-04	1.17E-04
⁶⁴ Ni	9.54E-14	1.56E-11	3.38E-12	2.46E-11	⁶⁴ Ni	1.82E-05	3.78E-05	4.87E-05	4.48E-05
⁶³ Cu	1.18E-05	8.19E-06	1.71E-05	2.06E-05	⁶³ Cu	1.46E-05	3.36E-05	3.88E-05	2.62E-05
⁶⁵ Cu	7.24E-07	6.00E-07	1.38E-06	1.86E-06	⁶⁵ Cu	7.79E-06	1.45E-05	2.08E-05	2.17E-05
⁶⁴ Zn	3.80E-04	2.64E-04	5.83E-04	6.88E-04	⁶⁴ Zn	3.33E-04	5.23E-04	7.85E-04	6.51E-04
⁶⁶ Zn	5.06E-06	2.59E-06	7.05E-06	6.90E-06	⁶⁶ Zn	1.72E-05	2.46E-05	4.10E-05	4.89E-05
⁶⁷ Zn	1.95E-07	6.07E-08	1.91E-07	1.18E-07	⁶⁷ Zn	1.68E-06	3.50E-06	4.84E-06	2.55E-06
⁶⁸ Zn	8.96E-08	1.21E-07	2.69E-07	4.86E-07	⁶⁸ Zn	7.85E-06	1.67E-05	2.49E-05	2.89E-05
⁷⁰ Zn	8.31E-14	1.95E-12	8.49E-13	1.95E-11	⁷⁰ Zn	2.42E-08	2.37E-08	1.08E-07	1.90E-07
⁶⁹ Ga	1.77E-08	2.11E-08	4.08E-08	8.95E-08	⁶⁹ Ga	1.21E-06	2.15E-06	3.84E-06	4.16E-06
⁷¹ Ga	1.54E-12	2.17E-11	3.79E-12	1.57E-10	⁷¹ Ga	8.48E-07	1.80E-06	3.02E-06	3.40E-06

$Z = 0.004$					$Z = 0.02$				
M	20	25	30	40	M	20	25	30	40
E	10	10	10	30	E	10	10	20	30
M_{cut}	2.20	1.96	3.98	4.41	M_{cut}	1.74	2.03	2.97	2.63
p	8.95E+00	1.02E+01	1.01E+01	1.03E+01	p	7.93E+00	8.41E+00	8.75E+00	3.55E+00
d	1.84E-13	2.01E-13	2.89E-13	3.88E-14	d	2.47E-13	1.97E-13	7.25E-13	1.43E-12
³ He	1.75E-04	1.85E-04	1.84E-04	1.80E-04	³ He	2.38E-04	2.21E-04	2.12E-04	5.05E-05
⁴ He	7.03E+00	8.49E+00	7.93E+00	8.12E+00	⁴ He	6.76E+00	7.25E+00	8.37E+00	4.78E+00
⁶ Li	6.12E-16	6.65E-16	9.58E-16	1.28E-16	⁶ Li	8.22E-16	6.56E-16	2.41E-15	4.75E-15
⁷ Li	4.31E-13	1.02E-13	8.01E-13	4.62E-12	⁷ Li	3.57E-12	5.29E-13	1.56E-14	5.72E-13
⁹ Be	6.27E-16	3.93E-16	1.88E-16	9.48E-18	⁹ Be	1.21E-16	1.85E-16	6.98E-16	2.43E-15
¹⁰ B	2.91E-11	3.09E-11	3.04E-11	6.57E-12	¹⁰ B	1.47E-10	1.51E-10	1.55E-10	7.44E-14
¹¹ B	2.79E-09	1.39E-10	1.37E-10	2.83E-11	¹¹ B	6.62E-10	6.79E-10	6.96E-10	3.80E-13
¹² C	8.32E-02	1.28E-01	1.36E-01	3.73E-01	¹² C	2.09E-01	1.44E-01	1.79E-01	4.90E-01
¹³ C	2.91E-04	3.83E-04	3.39E-04	3.68E-04	¹³ C	1.45E-03	6.65E-02	1.92E-03	4.31E-04
¹⁴ N	1.84E-02	3.15E-02	2.00E-02	2.52E-02	¹⁴ N	7.19E-02	8.43E-02	1.02E-01	5.81E-02
¹⁵ N	2.74E-05	9.45E-05	5.59E-06	1.35E-05	¹⁵ N	2.53E-04	4.63E-02	1.54E-05	4.26E-05
¹⁶ O	7.88E-01	2.07E+00	3.82E+00	6.80E+00	¹⁶ O	9.80E-01	2.18E+00	2.74E+00	7.05E+00
¹⁷ O	1.03E-04	1.12E-04	1.20E-04	1.57E-04	¹⁷ O	9.49E-04	1.34E-03	1.68E-03	9.69E-04
¹⁸ O	6.68E-04	7.80E-04	4.38E-05	6.51E-04	¹⁸ O	3.98E-03	8.37E-02	2.79E-03	1.04E-02
¹⁹ F	4.87E-06	8.48E-05	5.57E-06	8.50E-06	¹⁹ F	6.92E-05	1.18E-04	9.32E-06	9.84E-06
²⁰ Ne	1.42E-01	6.35E-01	4.92E-01	1.15E+00	²⁰ Ne	2.92E-01	6.47E-01	5.41E-01	1.74E+00
²¹ Ne	3.12E-04	3.57E-04	4.13E-04	8.62E-04	²¹ Ne	1.98E-03	1.70E-03	2.57E-03	5.19E-03
²² Ne	1.42E-03	4.54E-03	3.00E-03	7.99E-04	²² Ne	8.81E-03	1.66E-02	1.13E-02	1.07E-02
²³ Na	2.05E-03	4.68E-03	6.56E-03	1.32E-02	²³ Na	1.20E-02	1.41E-02	1.81E-02	5.76E-02
²⁴ Mg	8.10E-02	2.27E-01	1.91E-01	4.01E-01	²⁴ Mg	6.88E-02	2.08E-01	1.68E-01	3.29E-01
²⁵ Mg	1.64E-03	4.77E-03	4.94E-03	9.65E-03	²⁵ Mg	1.12E-02	2.42E-02	2.18E-02	5.82E-02
²⁶ Mg	1.69E-03	5.26E-03	5.62E-03	1.01E-02	²⁶ Mg	7.50E-03	2.11E-02	2.36E-02	5.93E-02
²⁷ Al	5.94E-06	7.44E-06	1.55E-05	3.07E-05	²⁷ Al	1.81E-05	6.23E-05	4.84E-05	9.70E-05
²⁸ Al	3.64E-03	1.04E-02	1.18E-02	2.29E-02	²⁸ Al	8.56E-03	2.34E-02	2.37E-02	7.20E-02
²⁸ Si	1.04E-01	1.22E-01	3.56E-01	5.74E-01	²⁸ Si	9.41E-02	1.24E-01	2.67E-01	3.28E-01
²⁹ Si	1.78E-03	2.27E-03	4.86E-03	6.63E-03	²⁹ Si	2.95E-03	8.30E-03	1.08E-02	1.70E-02
³⁰ Si	1.99E-03	2.32E-03	4.82E-03	7.37E-03	³⁰ Si	3.49E-03	1.10E-02	1.50E-02	1.97E-02
³¹ P	4.68E-04	5.29E-04	1.35E-03	2.00E-03	³¹ P	9.79E-04	1.99E-03	3.65E-03	5.43E-03
³² S	3.30E-02	4.02E-02	1.54E-01	2.30E-01	³² S	4.75E-02	4.35E-02	1.08E-01	1.40E-01
³³ S	2.93E-04	3.05E-04	1.05E-03	1.52E-03	³³ S	5.28E-04	6.07E-04	1.42E-03	1.73E-03
³⁴ S	1.39E-03	1.25E-03	4.79E-03	7.22E-03	³⁴ S	3.77E-03	4.36E-03	1.40E-02	1.69E-02
³⁶ S	5.15E-06	2.31E-06	8.74E-06	1.32E-05	³⁶ S	1.30E-05	2.23E-05	5.90E-05	8.41E-05
³⁵ Cl	7.46E-05	8.11E-05	2.90E-04	4.16E-04	³⁵ Cl	2.68E-04	1.58E-04	6.05E-04	8.23E-04
³⁷ Cl	2.39E-05	3.41E-05	1.06E-04	1.58E-04	³⁷ Cl	9.70E-05	1.40E-04	2.33E-04	5.21E-04
³⁶ Ar	4.40E-03	6.02E-03	2.28E-02	3.40E-02	³⁶ Ar	7.35E-03	6.63E-03	1.41E-02	1.98E-02
³⁸ Ar	4.28E-04	3.78E-04	1.78E-03	2.48E-03	³⁸ Ar	1.22E-03	5.80E-04	4.51E-03	5.14E-03
⁴⁰ Ar	1.46E-06	3.81E-07	2.87E-06	1.93E-06	⁴⁰ Ar	3.19E-06	3.30E-06	1.36E-05	8.04E-06
³⁹ K	4.32E-05	4.15E-05	1.72E-04	2.15E-04	³⁹ K	1.37E-04	6.78E-05	2.58E-04	2.56E-04
⁴⁰ K	2.25E-08	3.29E-08	8.55E-08	1.08E-07	⁴⁰ K	1.79E-07	2.25E-07	5.09E-07	9.26E-07
⁴¹ K	4.38E-06	4.66E-06	1.90E-05	2.32E-05	⁴¹ K	1.37E-05	1.11E-05	2.65E-05	4.65E-05
⁴⁰ Ca	3.06E-03	4.69E-03	1.67E-02	2.55E-02	⁴⁰ Ca	4.99E-03	5.67E-03	9.29E-03	1.42E-02
⁴² Ca	1.09E-05	9.19E-06	4.44E-05	5.81E-05	⁴² Ca	3.53E-05	1.34E-05	1.12E-04	1.24E-04
⁴³ Ca	1.09E-06	9.55E-07	1.12E-06	2.18E-06	⁴³ Ca	2.84E-06	3.57E-06	6.10E-06	7.56E-06
⁴⁴ Ca	2.86E-05	1.06E-04	1.12E-04	2.26E-04	⁴⁴ Ca	5.12E-05	9.93E-05	1.28E-04	4.13E-04
⁴⁶ Ca	2.35E-07	1.43E-07	6.94E-07	4.28E-07	⁴⁶ Ca	9.08E-07	1.33E-06	2.39E-06	3.71E-06
⁴⁸ Ca	1.07E-06	6.03E-07	9.78E-07	1.36E-06	⁴⁸ Ca	2.95E-06	2.77E-06	1.23E-05	2.69E-06
⁴⁵ Sc	6.08E-07	6.12E-07	1.52E-06	1.79E-06	⁴⁵ Sc	1.83E-06	2.71E-06	4.44E-06	6.81E-06
⁴⁶ Ti	4.52E-06	7.87E-06	1.99E-05	2.55E-05	⁴⁶ Ti	1.66E-05	7.32E-06	4.57E-05	5.62E-05
⁴⁷ Ti	1.57E-06	8.80E-06	1.22E-05	1.24E-05	⁴⁷ Ti	5.70E-06	8.09E-06	1.28E-05	3.99E-05
⁴⁸ Ti	4.89E-05	1.59E-04	2.30E-04	4.30E-04	⁴⁸ Ti	7.37E-05	1.66E-04	2.27E-04	5.93E-04
⁴⁹ Ti	1.49E-06	4.46E-06	6.49E-06	1.16E-05	⁴⁹ Ti	4.41E-06	8.24E-06	1.17E-05	1.84E-05
⁵⁰ Ti	8.29E-07	1.96E-06	2.54E-06	4.85E-06	⁵⁰ Ti	5.21E-06	1.06E-05	8.54E-06	3.31E-05
⁵⁰ V	1.02E-08	2.02E-08	4.10E-08	7.58E-08	⁵⁰ V	5.94E-08	1.40E-07	3.68E-07	3.69E-07
⁵¹ V	3.17E-06	2.26E-05	2.18E-05	2.74E-05	⁵¹ V	1.09E-05	1.55E-05	2.48E-05	6.58E-05
⁵⁰ Cr	1.49E-05	2.05E-05	5.69E-05	8.03E-05	⁵⁰ Cr	7.07E-05	2.02E-05	9.87E-05	1.21E-04
⁵² Cr	2.69E-04	8.48E-04	1.71E-03	3.28E-03	⁵² Cr	4.11E-04	9.25E-04	1.45E-03	2.47E-03
⁵³ Cr	2.14E-05	5.36E-05	1.06E-04	1.99E-04	⁵³ Cr	5.54E-05	7.52E-05	1.34E-04	1.44E-04
⁵⁴ Cr	2.34E-06	5.15E-06	5.76E-06	9.29E-06	⁵⁴ Cr	1.48E-05	2.42E-05	3.72E-05	4.99E-05
⁵⁵ Mn	9.05E-05	1.67E-04	3.26E-04	5.81E-04	⁵⁵ Mn	3.18E-04	3.53E-04	5.85E-04	4.94E-04
⁵⁴ Fe	8.16E-04	1.17E-03	3.00E-03	4.97E-03	⁵⁴ Fe	3.79E-03	2.12E-03	4.03E-03	5.89E-03
⁵⁶ Fe	3.11E-02	8.32E-02	1.53E-01	2.73E-01	⁵⁶ Fe	3.57E-02	8.87E-02	1.04E-01	2.77E-01
⁵⁷ Fe	9.93E-04	1.93E-03	3.31E-03	6.26E-03	⁵⁷ Fe	1.22E-03	2.83E-03	4.11E-03	8.90E-03
⁵⁸ Fe	5.48E-05	1.62E-04	1.77E-04	2.84E-04	⁵⁸ Fe	4.24E-04	7.36E-04	1.76E-03	1.36E-03
⁵⁹ Co	4.90E-05	3.67E-04	3.31E-04	4.47E-04	⁵⁹ Co	2.43E-04	4.22E-04	6.60E-04	1.42E-03
⁵⁸ Ni	3.00E-04	9.15E-04	9.42E-04	1.51E-03	⁵⁸ Ni	1.52E-03	2.12E-03	3.37E-03	7.14E-03
⁶⁰ Ni	1.01E-03	2.97E-03	4.92E-03	8.28E-03	⁶⁰ Ni	1.20E-03	3.14E-03	3.33E-03	1.12E-02
⁶¹ Ni	1.50E-04	9.23E-05	2.93E-04	3.60E-04	⁶¹ Ni	2.43E-04	2.97E-04	9.10E-04	8.55E-04
⁶² Ni	1.23E-04	1.72E-04	2.78E-04	6.21E-04	⁶² Ni	3.69E-04	8.87E-04	8.34E-04	2.97E-03
⁶⁴ Ni	1.66E-05	8.07E-05	1.10E-04	2.66E-04	⁶⁴ Ni	1.60E-04	5.10E-04	6.97E-05	1.95E-03
⁶³ Cu	8.84E-06	4.23E-05	4.77E-05	9.13E-05	⁶³ Cu	9.89E-05	2.32E-04	6.14E-05	5.85E-04
⁶⁵ Cu	7.52E-06	2.84E-05	4.86E-05	1.12E-04	⁶⁵ Cu	4.15E-05	1.34E-04	2.02E-05	5.70E-04
⁶⁴ Zn	3.63E-05	3.19E-04	3.56E-04	5.84E-04	⁶⁴ Zn	5.27E-05	1.35E-04	8.32E-05	6.38E-04
⁶⁶ Zn	2.10E-05	4.85E-05	1.08E-04	2.13E-04	⁶⁶ Zn	7.13E-05	2.35E-04	7.40E-05	1.02E-03
⁶⁷ Zn	1.45E-06	7.12E-06	1.14E-05	2.81E-05	⁶⁷ Zn	1.17E-05	4.38E-05	3.01E-06	2.31E-04
⁶⁸ Zn	7.86E-06	3.70E-05	7.55E-05	1.84E-04	⁶⁸ Zn	5.33E-05	2.75E-04	1.19E-05	1.43E-03
⁷⁰ Zn	2.39E-07	1.97E-07	1.33E-06	2.98E-06	⁷⁰ Zn	2.45E-06	8.48E-06	5.89E-07	5.62E-05
⁶⁹ Ga	1.36E-06	5.39E-06	1.49E-05	3.43E-05	⁶⁹ Ga	6.82E-06	2.69E-05	1.27E-06	1.61E-04
⁷¹ Ga	1.10E-06	3.95E-06	9.36E-06	2.16E-05	⁷¹ Ga	4.95E-06	2.39E-05	2.26E-06	1.29E-04

Table 3

The IMF weighted yields with $x = 1.35$, $M_\ell = 0.07M_\odot$, $M_u = 50M_\odot$.

Z	SNII+HN			
	0	0.001	0.004	0.02
p	3.28E-02	3.14E-02	2.96E-02	2.45E-02
d	5.76E-18	2.21E-15	1.97E-16	5.34E-16
³ He	2.51E-07	5.24E-07	6.52E-07	7.06E-07
⁴ He	2.30E-02	2.26E-02	2.22E-02	2.05E-02
⁶ Li	1.70E-20	1.52E-19	6.49E-19	1.76E-18
⁷ Li	8.67E-12	6.67E-13	3.14E-15	5.85E-14
⁹ Be	1.25E-20	7.74E-19	6.54E-19	7.26E-19
¹⁰ B	1.86E-17	2.38E-14	1.47E-13	4.25E-13
¹¹ B	5.00E-16	1.05E-13	1.12E-11	1.83E-12
¹² C	7.51E-04	4.14E-04	5.17E-04	6.75E-04
¹³ C	1.75E-10	4.33E-07	2.80E-05	3.06E-05
¹⁴ N	3.36E-06	2.82E-05	8.77E-05	2.35E-04
¹⁵ N	5.17E-10	1.35E-08	2.41E-05	1.90E-05
¹⁶ O	8.03E-03	8.05E-03	6.58E-03	6.14E-03
¹⁷ O	3.45E-09	1.42E-07	8.36E-07	3.60E-06
¹⁸ O	5.69E-09	2.24E-06	2.70E-05	5.29E-05
¹⁹ F	3.49E-11	6.76E-09	4.98E-08	1.08E-07
²⁰ Ne	1.28E-03	1.38E-03	1.57E-03	1.68E-03
²¹ Ne	1.05E-07	6.66E-07	1.62E-06	4.95E-06
²² Ne	7.53E-08	3.39E-06	8.01E-06	2.79E-05
²³ Na	4.46E-06	8.18E-06	2.03E-05	5.41E-05
²⁴ Na	5.69E-04	6.69E-04	4.88E-04	4.06E-04
²⁵ Mg	9.62E-07	5.62E-06	1.59E-05	6.08E-05
²⁶ Mg	9.19E-07	5.04E-06	1.57E-05	5.68E-05
²⁷ Al	1.27E-05	2.49E-05	2.95E-05	6.53E-05
²⁸ Si	8.11E-04	7.09E-04	6.17E-04	4.55E-04
²⁹ Si	3.03E-06	5.90E-06	7.62E-06	1.88E-05
³⁰ Si	3.40E-06	7.40E-06	9.24E-06	2.12E-05
³¹ P	1.28E-06	2.34E-06	2.14E-06	5.54E-06
³² S	3.12E-04	2.86E-04	2.50E-04	1.96E-04
³³ S	8.06E-07	1.03E-06	1.17E-06	1.62E-06
³⁴ S	1.70E-06	3.20E-06	6.09E-06	1.31E-05
³⁶ S	3.84E-11	1.98E-09	1.48E-08	8.19E-08
³⁵ Cl	2.18E-07	3.34E-07	3.49E-07	7.91E-07
³⁷ Cl	8.78E-08	8.89E-08	1.50E-07	4.89E-07
³⁶ Ar	4.54E-05	4.21E-05	3.80E-05	3.03E-05
³⁸ Ar	8.47E-07	1.11E-06	2.29E-06	4.51E-06
⁴⁰ Ar	2.42E-13	4.64E-10	3.34E-09	1.02E-08
³⁹ K	1.16E-07	1.41E-07	2.08E-07	3.41E-07
⁴⁰ K	1.39E-11	6.81E-11	1.29E-10	7.86E-10
⁴¹ K	2.25E-08	1.92E-08	2.25E-08	4.91E-08
⁴⁰ Ca	3.58E-05	3.34E-05	3.02E-05	2.39E-05
⁴² Ca	1.95E-08	2.95E-08	5.48E-08	1.12E-07
⁴³ Ca	2.58E-10	1.30E-09	3.25E-09	9.89E-09
⁴⁴ Ca	1.50E-07	1.74E-07	1.61E-07	2.65E-07
⁴⁶ Ca	5.69E-14	2.06E-10	8.71E-10	3.60E-09
⁴⁸ Ca	8.04E-15	6.91E-10	2.93E-09	1.07E-08
⁴⁵ Sc	6.48E-10	1.26E-09	2.55E-09	7.59E-09
⁴⁶ Ti	2.02E-08	2.61E-08	3.03E-08	5.11E-08
⁴⁷ Ti	2.71E-08	2.70E-08	1.84E-08	2.80E-08
⁴⁸ Ti	4.58E-07	4.98E-07	4.97E-07	5.70E-07
⁴⁹ Ti	1.56E-08	1.77E-08	2.09E-08	3.07E-08
⁵⁰ Ti	1.52E-14	2.04E-09	7.64E-09	3.16E-08
⁵⁰ V	2.88E-13	5.92E-11	9.07E-11	3.42E-10
⁵¹ V	6.03E-08	5.76E-08	5.09E-08	6.13E-08
⁵⁰ Cr	1.14E-07	1.12E-07	1.33E-07	1.72E-07
⁵² Cr	5.45E-06	5.51E-06	5.76E-06	5.06E-06
⁵³ Cr	3.17E-07	3.30E-07	3.68E-07	3.81E-07
⁵⁴ Cr	2.73E-11	5.57E-09	1.84E-08	7.09E-08
⁵⁵ Mn	8.72E-07	9.72E-07	1.16E-06	1.54E-06
⁵⁴ Fe	7.32E-06	8.34E-06	9.03E-06	1.13E-05
⁵⁶ Fe	3.17E-04	3.38E-04	3.22E-04	3.48E-04
⁵⁷ Fe	4.66E-06	6.03E-06	6.79E-06	9.57E-06
⁵⁸ Fe	6.15E-12	1.81E-07	5.26E-07	2.15E-06
⁵⁹ Co	6.82E-07	6.72E-07	7.47E-07	1.20E-06
⁵⁸ Ni	1.96E-06	3.12E-06	1.22E-05	8.12E-06
⁶⁰ Ni	8.03E-06	8.48E-06	7.61E-06	9.46E-06
⁶¹ Ni	1.26E-07	2.17E-07	4.20E-07	8.15E-07
⁶² Ni	7.54E-08	4.66E-07	1.81E-06	2.12E-06
⁶⁴ Ni	1.01E-14	8.66E-08	2.89E-07	1.36E-06
⁶³ Cu	2.08E-08	4.44E-08	1.10E-07	5.07E-07
⁶⁵ Cu	1.36E-09	3.25E-08	1.05E-07	3.84E-07
⁶⁴ Zn	6.32E-07	5.74E-07	5.07E-07	4.43E-07
⁶⁶ Zn	5.80E-09	6.24E-08	2.03E-07	6.65E-07
⁶⁷ Zn	1.45E-10	6.43E-09	2.75E-08	1.43E-07
⁶⁸ Zn	2.67E-10	4.31E-08	1.67E-07	8.69E-07
⁷⁰ Zn	5.14E-15	3.62E-10	1.85E-09	2.63E-08
⁶⁹ Ga	4.93E-11	5.26E-09	2.45E-08	9.57E-08
⁷¹ Ga	4.22E-14	4.81E-09	1.87E-08	7.68E-08
⁷⁰ Ge	3.67E-11	9.13E-09	3.62E-08	1.45E-07
⁷² Ge	2.34E-14	1.13E-08	5.05E-08	2.44E-07
⁷³ Ge	2.83E-14	1.28E-09	8.59E-09	5.62E-08
⁷⁴ Ge	1.33E-14	2.18E-08	1.35E-07	7.93E-07

References

- [1] Abel, T., Bryan, G.L., & Norman, M.L., *Science* **295** (2002) 93
- [2] Aoki, W., Norris, J. E., Ryan, S. G., Beers, T. C., Christlieb, N., Tsangarides, S., & Ando, H., *ApJ* **608** (2004) 971
- [3] Aoki, W., Frebel, A., Christlieb, N., et al., *ApJ* **639** (2006) 897
- [4] Argast, D., Samland, M., Gerhard, O.E., & Thielemann, F.-K., *A&A* **356** (2000) 873
- [5] Arnett, W.D., *Supernovae and Nucleosynthesis* (Princeton Univ. Press) (1996)
- [6] Asplund, M. *ARA&A* **43** (2005) 481
- [7] Audouze, J., & Silk, J., *ApJ* **451** (1995) L49
- [8] Baraffe, I., Heger, A., & Woosley, S.E., *ApJ* **550** (2001) 890
- [9] Beers, T., & Christlieb, N., *ARA&A* **43** (2005) 531
- [10] Bensby, T., Feltzing, S., & Lundstrom, I., *A&A* **410** (2003) 527
- [11] Bessell, M.S., Christlieb, N., & Gustafsson, B., *ApJ* **612** (2004) L61
- [12] Bromm, V., & Larson, R., *ARA&A* **42** (2004) 79
- [13] Burrows, A., Livne, E., Dessart, L., Ott, C.D., & Murphy, J., *ApJ* **640** (2006) 878
- [14] Campana, S., et al., *Nature* (2006) submitted (astro-ph/0603279)
- [15] Cayrel, R., et al., *A&A* **416** (2004) 1117
- [16] Chieffi, A., & Limongi, M., *ApJ* **577** (2002) 281
- [17] Christlieb, N., et al., *Nature* **419** (2002) 904
- [18] Christlieb, N., et al., *ApJ* **603** (2004) 708
- [19] Christlieb, N., in *ESO/MPA workshop, Carbon-rich Ultra Metal-Poor Stars of the Galactic Halo*, ed. A. Weiss & F. Primas (MPA) (2005)
- [20] Edvardsson, B., Andersen, J., Gustafsson, B., Lambert, D.L., Nissen, P.E., & Tomkin, J., *A&A* **275** (1993) 101
- [21] Filippenko, A.V., *ARA&A* **35** (1997) 309
- [22] Francois, P., Matteucci, F., Cayrel, R., Spite, M., Spite, F., & Chaippini, C., *A&A* **421** (2004) 613
- [23] Frebel, A., et al., *Nature* **434** (2005) 871
- [24] Frebel, A., Christlieb, N., Norris, J.E., Aoki, W., & Asplund, M., *ApJ* **638** (2006) L17
- [25] Fröhlich, C., Hauser, P., Liebendörfer, M., Martínez-Pinedo, G., Thielemann, F.-K., Bravo, E., Zinner, N. T., Hix, W. R., Langanke, K., Mezzacappa, A., & Nomoto, K., *ApJ* **637** (2006) 415
- [26] Fröhlich, C., Martínez-Pinedo, G., Liebendörfer, M., Thielemann, F.-K., et al., *Phys Rev Let* **96** (2006) 142502
- [27] Fryer, C.L., Woosley, S. E., & Heger, A., *ApJ* **550** (2001) 372
- [28] Fryer, C.L. (ed.) *Stellar Collapse* (Astrophysics and Space Science Library: Kluwer) (2004)
- [29] Fusco-Femiano, R., & Matteucci, F. (ed.), *ASP Series 253 Chemical Enrichment of Intracluster and Intergalactic Medium*, (ASP) (2002)
- [30] Galama, T., et al., *Nature* **395** (1998) 670

- [31] Gratton, R.G., et al., *A&A* **404** (2003) 187
- [32] Hachisu, I., Matsuda, T., Nomoto, K., et al., *ApJ* **358** (1990) L57
- [33] Hamuy, M., *ApJ* **582** (2003) 905
- [34] Heger, A., & Langer, N., *ApJ* **544** (2000) 1016
- [35] Heger, A., & Woosley, S.E., *ApJ* **567** (2002) 532
- [36] Hill, V., Francois, P., & Primas, F. (ed.), *IAU Symp 228, From Lithium to Uranium* (Cambridge Univ. Press) (2005)
- [37] Hillebrandt, W., & Leibundgut, B. (ed.), *From Twilight to Highlight: The Physics of Supernovae* (Springer) (2003)
- [38] Hjorth, J., et al., *Nature* **423** (2003) 847
- [39] Honda, S. et al., *ApJ* **607** (2004) 474
- [40] Ibrahim, A., Boury, A., & Noels, A., *A&A* **103** (1981) 390
- [41] Israelian, G. & Reboro, R., *ApJ* **557** (2001) L43
- [42] Iwamoto, K., Mazzali, P.A., Nomoto, K., et al., *Nature* **395** (1998) 672
- [43] Iwamoto, K., Brachwitz, F., Nomoto, K., Kishimoto, N., Umeda, H., Hix, W. R., & Thielemann, F-K., *ApJS* **125** (1999) 439
- [44] Iwamoto, K., Nakamura, T., Nomoto, K., et al., *ApJ* **534** (2000) 660
- [45] Iwamoto, N., Umeda, H., Tominaga, N., Nomoto, K., & Maeda, K., *Science* **309** (2005) 451
- [46] Janka, H.-Th. *A&A* **368** (2001) 527
- [47] Kawabata, K., et al., *ApJ* **580** (2002) L39
- [48] Kifonidis, K., Plewa, T., Janka, H.-Th., et al., *A&A* **408** (2003) 621
- [49] Kobayashi, C., Tsujimoto, T., Nomoto, K., Hachisu, I., & Kato, M., *ApJ* **503** (1998) L155
- [50] Kobayashi, C., Tsujimoto, T., & Nomoto, K., *ApJ* **539** (2000) 26
- [51] Kobayashi, C., in *IAU Symp 228, From Lithium to Uranium*, ed. V. Hill et al. (Cambridge Univ. Press) (2005) 297 (astro-ph/0508000)
- [52] Kobayashi, C., Umeda, H., Nomoto, K., Tominaga, N., & Ohkubo, T., *ApJ* (2006) submitted
- [53] Langer, N., *A&A* **265** (1992) L17
- [54] Liebendörfer, M., Mezzacappa, A., Messer, O. E. B., Martinez-Pinedo, G., Hix, W. R., Thielemann, F.-K., *Nuclear Phys A* **719** (2003) 144
- [55] Liebendörfer, M., Rampp, M., Janka, H.-Th., & Mezzacappa, A., *ApJ* **620** (2005) 840
- [56] Limongi, M., & Chieffi, A., *ApJ* **592** (2003) 404
- [57] Limongi, M., Chieffi, A., & Bonifacio, P., *ApJ* **594** (2003) L123
- [58] Maeda, K., Nakamura, T., Nomoto, K., Mazzali, P.A., Patat, F., & Hachisu, I. *ApJ* **565** (2002) 405
- [59] Maeda, K. & Nomoto, K., *ApJ* **598** (2003) 1163
- [60] Maeda, K., in *Origin of Matter and Evolution of Galaxies* (2006) ed. S. Kubono et al. (AIP), in press
- [61] Maeder, A. & Meynet, G., *ARA&A* **38** (2000) 143
- [62] Malesani, J., et al., *ApJ* **609** (2006) L5
- [63] Matteucci, F., *The Chemical Evolution of the Galaxy* (Kluwer Academic Pub.) (2001)

- [64] Mazzali, P.A., Iwamoto, K., Nomoto, K., *ApJ* **545** (2000) 407
- [65] Mazzali, P.A., Deng, J., Maeda, K., Nomoto, K., et al., *ApJ* **572** (2002) L61
- [66] Mazzali, P.A., et al., *ApJ* **599** (2003) L95
- [67] Mazzali, P.A., Deng, J., Nomoto, K., et al., *Nature* (2006) submitted (astro-ph/0603567)
- [68] McWilliam, A., Preston, G.W., Sneden, C., et al., *AJ* **109** (1995) 2757
- [69] Melendez, J. & Barbuy, B., *ApJ* **575** (2002) 474
- [70] Meynet, G., Ekstrom, S., & Maeder, A., *A&A* **447** (2006) 623
- [71] Nagataki, S., *ApJS* **127** (2000) 141
- [72] Nakamura, T., Umeda, H., Nomoto, K., Thielemann, F.-K., & Burrows, A., *ApJ* **517** (1999) 193
- [73] Nakamura, T., Mazzali, P.A., Nomoto, K., Iwamoto, K., *ApJ* **550** (2001a) 991
- [74] Nakamura, T., Umeda, H., Iwamoto, K., Nomoto, K., et al., *ApJ* **555** (2001b) 880
- [75] Nissen, P.E., Primas, F., Asplund, M., & Lambert, D.L., *A&A* **390** (2002) 235
- [76] Nomoto, K., Yamaoka, H., Shigeyama, T., Kumagai, S., & Tsujimoto, T., in *Supernovae*, Les Houche Session LIV (1994) ed. S. Bludmann et al. (North-Holland) 199
- [77] Nomoto, K., Shigeyama, T., Kumagai, S., Yamaoka, H., & Suzuki, T., in *Supernovae*, Les Houche Session LIV (1994) ed. S. Bludmann et al. (North-Holland) 489
- [78] Nomoto, K., Yamaoka, H., Pols, O.R., van den Heuvel, E.P.J., et al., *Nature* **371** (1994) 227
- [79] Nomoto, K., Hashimoto, M., Tsujimoto, T., Thielemann, F.-K., et al., *Nuclear Phys* **A616** (1997) 79c
- [80] Nomoto, K., Mazzali, P.A., Nakamura, T., et al., in *Supernovae and Gamma Ray Bursts*, eds. M. Livio et al. (Cambridge Univ. Press) (2001) 144 (astro-ph/0003077)
- [81] Nomoto, K., Maeda, K., Umeda, H., et al., in *IAU Symp 212, A Massive Star Odyssey, from Main Sequence to Supernova*, eds. V.D. Hucht, et al. (San Francisco: ASP) (2003) 395 (astro-ph/0209064)
- [82] Nomoto, K., Maeda, K., Mazzali, P.A., et al., in *Stellar Collapse*, ed. C.L. Fryer (Astrophysics and Space Science Library: Kluwer) (2004) 277 (astro-ph/0308136)
- [83] Nomoto, K., Tominaga, N., Umeda, H., & Kobayashi, C., in *IAU Symp 228, From Lithium to Uranium*, ed. V. Hill et al. (Cambridge Univ. Press) (2005) 287 (astro-ph/0603433)
- [84] Norris, J.E., Ryan, S.G., & Beers, T.C., *ApJ* **561** (2001) 1034
- [85] Ohkubo, T., Umeda, H., Maeda, K., Nomoto, K., Suzuki, T., Tsuruta, S., & Rees, M.J., *ApJ* **654** (2006) in press (astro-ph/0507593)
- [86] Paczyński, B., *ApJ* **494** (1998) L45
- [87] Pagel, B.E.J., *Nucleosynthesis and Chemical Evolution of Galaxies*

- (Cambridge Univ. Press) (1997)
- [88] Pian, E., et al., *Nature* (2006) submitted (astro-ph/0603530)
 - [89] Primas, F., et al., in *The First Stars* (2000), ed. A. Weiss, T. Abel, & V. Hill (Berlin: Springer), 51
 - [90] Pruet, J., Woosley, S.E., Buras, R., Janka, H.-T., & Hoffman, R.D., *ApJ* **623** (2005) 325
 - [91] Qian, Y.-Z., & Wasserburg, G.J., *ApJ* **635** (2005) 845
 - [92] Rampp, M., & Janka, H.-Th., *ApJ* **539** (2000) L33
 - [93] Rauscher, T., Heger, A., Hoffman, R.D., & Woosley, S.E., *ApJ* **576** (2002) 323
 - [94] Ryan, S.G., Norris, J.E., & Beers, T.C., *ApJ* **471** (1996) 254
 - [95] Schneider, R., Ferrara, A., Salvaterra, R., Omukai, K., & Bromm, V., *Nature* **422** (2003) 869
 - [96] Shigeyama, T., & Tsujimoto, T., *ApJ* **507** (1998) L135
 - [97] Sneden, C., Gratton, R.G., & Crocker, D.A., *A&A* **246** (1991) 354
 - [98] Sollerman, J., Cumming, R., & Lundqvist, P., *ApJ* **493** (1998) 933
 - [99] Stanek, K.Z., et al., *ApJ* **591** (2003) L17
 - [100] Suda, T., Aikawa, M., Machida, M.N., Fujimoto, M.Y., & Iben, I., Jr., *ApJ* **611** (2004) 476
 - [101] The, L.-S., Clayton, D.D., Diehl, R., et al., *A&A* **450** (2006) 1037
 - [102] Thielemann, F.-K., Nomoto, K., & Hashimoto, M., *ApJ* **460** (1996) 408
 - [103] Tominaga, N., Tanaka, M., Nomoto, K., et al., *ApJ* **633** (2005) L97
 - [104] Tominaga, N., Umeda, H., & Nomoto, K. *ApJ* (2006) submitted
 - [105] Tumlinson, J., *ApJ* **641** (2006) 1
 - [106] Tumlinson, J., Venkatesan, A., & Shull, M., *ApJ* **612** (2004) 602
 - [107] Turatto, M., Mazzali, P.A., Young, T., Nomoto, K., et al., *ApJ* **498** (1998) L129
 - [108] Umeda, H. Nomoto, K., & Nakamura, T., in *The First Stars* (2000), ed. A. Weiss, T. Abel, & V. Hill (Berlin: Springer), 150 (astro-ph/9912248)
 - [109] Umeda, H., & Nomoto, K., *ApJ* **565** (2002) 385
 - [110] Umeda, H., Nomoto, K., Tsuru, T., et al., *ApJ* **578** (2002) 855
 - [111] Umeda, H., & Nomoto, K., *Nature* **422** (2003) 871
 - [112] Umeda, H. & Nomoto, K., *ApJ* **619** (2005) 427
 - [113] Wanajo, S., *ApJ* (2006) in press (astro-ph/0602488)
 - [114] Wang, L., Baade, D., Höflich, P., & Wheeler, J.C., *ApJ* **592** (2003) 457
 - [115] Wasserburg, G.J., & Qian, Y.-Z., *ApJ* **529** (2000) L21
 - [116] Weiss, A., Abel, T., & Hill, V. (eds.), *The First Stars* (Berlin: Springer) (2000)
 - [117] Weiss, A., Schlattl, H., Salaris, M., et al., *A&A* bf 422 (2004) 217
 - [118] Woosley, S.E., *ApJ* **405** (1993) 273
 - [119] Woosley, S.E., & Bloom, J., *ARA&A* **44** (2006) in press
 - [120] Woosley, S.E., & Weaver, T.A., *ApJS* **101** (1995) 181
 - [121] Yoshii, Y., *A&A* **97** (1981) 280
 - [122] Zampieri, L., et al., *MNRAS* **338** (2003) 711